International Journal of Biological Macromolecules 330 (2025) 148058

Contents lists available at ScienceDirect

International Journal of Biological Macromolecules

journal homepage: www.elsevier.com/locate/ijbiomac

Incorporation of monophosphoryl lipid A and CpG-oligodeoxynucleotides into lipid nanoparticles activates toll-like receptor signaling pathways while maintaining antigen expression for mRNA-based vaccinations

Ana Pena Vaquero [a], Paula Calderon-Ruiz [a], Rocio Gambaro [a], Ignacio Rivero-Berti [a,b], María-José Limeres [a], Silvia Fraude-El Ghazi [a], Cristián Huck-Iriart [c], Claudius U. Meyer [a], Maximiliano L. Cacicedo [a], Thomas Hankeln [d], Shutian Si [e], Ingo Lieberwirth [e], Katharina Landfester [e], Catalina Alba Soto [f], Valeria Tekiel [g], Matthias Bros [h], Stephan Gehring [a,*], German A. Islan [a,b,*]

[a] Children's Hospital, University Medical Center Mainz, Mainz, Germany
[b] CINDEFI (UNLP-CONICET), La Plata, Buenos Aires, Argentina
[c] ALBA Synchrotron Light Source, Cerdanyola del Vallès, 08290, Barcelona, Spain
[d] Institute of Organismic and Molecular Evolution, Faculty of Biology, Johannes Gutenberg-University, Mainz, Germany
[e] Max Planck Institute for Polymer Research, Department of Physical Chemistry of Polymers, Mainz, Germany
[f] Departamento de Microbiología, Parasitología e Inmunología, Facultad de Medicina, Universidad de Buenos Aires, Instituto de Investigaciones en Microbiología y Parasitología Médicas (IMPaM), UBA-CONICET, Buenos Aires, Argentina
[g] Instituto de Investigaciones Biotecnológicas, Escuela de Bio y nanotecnologías (EByN), Universidad Nacional de San Martín (UNSAM), Consejo Nacional de Investigaciones Científicas y Técnicas (CONICET), San Martín, Buenos Aires, Argentina
[h] Department of Dermatology, University Medical Center, Langenbeckstr. 1, 55131, Mainz, Germany

ARTICLE INFO

Keywords:
Lipid nanoparticles
mRNA delivery
Adjuvants
Cytokines
MPLA
CpG-ODN
Innate immune response

ABSTRACT

Lipid nanoparticles (LNPs) were engineered for efficient mRNA delivery and immune enhancement through co-encapsulation of adjuvants. CpG-oligodeoxynucleotides (CpG-ODN, TLR9 agonist) and monophosphoryl lipid A (MPLA, TLR4 agonist) were incorporated to activate intra- and extracellular Toll-like receptor pathways. Formulated *via* microfluidics, CpG was added in the aqueous phase and MPLA in the lipid phase. The final LNP-MPLA-CpG formulation included Luc mRNA and CpG-ODN (5:1 ratio) with ALC-0315/DSPC/cholesterol/ALC-0159/MPLA (1 %). Particle characterization by DLS and NTA confirmed neutral, homogeneous nanoparticles (~80 nm). Cryo-TEM and SAXS verified structural integrity. The formulation maintained over 80 % mRNA encapsulation after storage at 4 °C and − 80 °C. Transfection of human and murine dendritic cells (MoDCs and DC2.4) led to robust protein expression. The LNPs showed minimal hemotoxicity and low cytotoxicity, while significantly increasing pro-inflammatory cytokines (IFN-γ, TNF-α, IL-6) in both cell types. DC uptake of LNP-MPLA-CpG was efficient. In the *in vivo* biodistribution, Luc mRNA was primarily expressed in liver and spleen following intramuscular injection. Serum cytokine levels peaked at 6 h post-injection, and flow cytometry of stimulated splenocytes and liver non-parenchymal cells confirmed a strong innate activation. These results support LNP co-delivery of dual adjuvants as a potent platform for enhancing mRNA vaccine efficacy and innate immune activation.

1. Introduction

The rapid development of mRNA vaccines during the COVID-19 pandemic has significantly increased interest in lipid nanoparticles (LNPs), establishing them as a powerful platform for efficient RNA intracellular delivery [1]. LNPs typically comprise four main lipid components: ionizable lipids, phospholipids, cholesterol, and polyethylene glycol (PEG) [2]. To date, three RNA/LNP-based drugs have been approved by the U.S. Food and Drug Administration (FDA) and are commercially available. These include Onpattro®, an siRNA treatment

* Corresponding authors at: Children's Hospital, University Medical Center Mainz, Mainz, Germany
E-mail addresses: stephan.gehring@uni-mainz.de (S. Gehring), germanis@uni-mainz.de (G.A. Islan).

https://doi.org/10.1016/j.ijbiomac.2025.148058
Received 26 May 2025; Received in revised form 4 August 2025; Accepted 30 September 2025
Available online 1 October 2025

for transthyretin-mediated amyloidosis, followed by Moderna's Spikevax® and Pfizer/BioNTech's Comirnaty® COVID-19 mRNA vaccines, all of which have demonstrated the potential of RNA-based drugs. Meanwhile, there are numerous ongoing clinical trials exploring novel LNP-formulated mRNA vaccines, reflecting the growing pharmaceutical interest in this technology. However, further research is required to elucidate both the beneficial and adverse immunological effects, upon which tailored formulations with specific profiles can be developed [3].

Adjuvants are essential components of vaccines, playing a critical role in enhancing immune responses. However, several challenges persist, including potential side effects which limits the introduction of novel adjuvants into the clinic. Targeted delivery of adjuvants to professional antigen-presenting cells (APCs) offers a promising strategy to reduce the required adjuvant dose while simultaneously promoting sustained antigen expression and adjuvant-driven maturation of dendritic cells (DCs) [4–6].

In general, mRNA vaccine responses can be enhanced through two main approaches: the use of adjuvants acting as immunostimulants and through optimized delivery systems [7]. Adjuvants induce the activation of APCs by acting as danger signal molecules. They interact with pattern recognition receptors (PRRs), such as Toll-like receptors (TLRs), which in turn amplify the adaptive immune responses by facilitating the antigen presentation and induction of co-stimulatory signals, concomitant with the production of pro-inflammatory cytokines. In contrast, delivery systems improve the immune response by increasing antigen load, resulting in prolonged bioavailability of antigens and enhancing their targeted delivery to lymph nodes and APCs, thereby boosting the overall efficiency of immune response [7].

The selection of adjuvants and nano-carrier formulations depends on various factors, including the physicochemical properties of the vaccine antigen (*i.e.* mRNA-encoded *versus* protein-based), the stability of the adjuvant, its hydrophobic/hydrophilic nature, the type of immune response required for the target pathology and the potential route of administration. Selection of an inappropriate adjuvant could compromise the efficacy of a vaccine antigen, *e.g.* by inducing a cytokine storm or suppressing mRNA expression [8–10].

TLRs are a family of PRRs that recognize conserved microbial components and play a critical role in innate immunity [11]. TLR agonists are widely used as natural immune adjuvants and have been extensively explored in the context of vaccine development and immunotherapy for various infectious and cancer-related diseases [12]. Among these, lipopolysaccharide (LPS), a component of the outer membrane of Gram-negative bacteria, and its less toxic synthetic derivative, monophosphoryl lipid A (MPLA), are particularly interesting immunostimulatory candidates [13]. MPLA activates APCs by binding to and activating TLR4 which is located on the cell surface. This activation promotes a predominantly T helper 1 (Th1)-biased immune response following vaccination [14].

Synthetic oligodeoxynucleotides (ODNs) containing immunostimulatory CpG motifs represent another promising candidate for enhancing vaccine efficacy. CpG-ODNs activate TLR9, which is located within intracellular vesicles, triggering an immunomodulatory cascade that involves natural killer (NK) cells and professional APCs, such as DCs and monocyte/macrophages. This activation promotes a Th1-biases immune response and induces the secretion of pro-inflammatory cytokines, thereby enhancing antigen-specific T and B cell responses. Consistent with this findings, several studies have demonstrated that CpG-ODNs enhance the immunogenicity of co-administered vaccines [15,16]. However, the therapeutic potential of soluble CpG-ODNs is limited by hepatic toxicity and insufficient immune activation in draining lymph nodes. Notably, the FDA recently approved CpG 1018 as the first CpG-based adjuvant licensed for a human Hepatitis B vaccine (HEPLISAV-B) [17]. While clinical trials have demonstrated its safety and efficacy, CpG ODNs are typically administered in soluble form, leading to a rapid diffusion from the injection site into systemic circulation. This results in an unintended off-target activation of the innate immune system and hepatocyte apoptosis, significantly reducing the therapeutic applicability of CpG ODNs [18].

To overcome these limitations, B-class CpG ODN1826, suitable for activation of B cells and induction of IL-6 release, has been incorporated within LNPs in which the ionizable cationic lipid binds CpG through electrostatic interactions. When administered locally, LNP-formulated CpG efficiently drains to lymph nodes and triggers robust innate immune activation, a result not observed with soluble CpG [19]. Moreover, a study demonstrated that encapsulating a CpG ODN within LNPs at a dose of 10.88 μg could enhance the therapeutic vaccine efficiency [20].

Various mRNA-based vaccine platforms have been investigated, highlighting the importance of evaluating key parameters such as mRNA delivery efficiency, tolerability, and immunogenicity to clearly understand the suitability of formulating adjuvants into LNPs. Some reports have explored the use of nanoparticle-delivered adjuvants to enhance cellular immunity such as the inclusion of α-galactosylceramide into LNPs [21], MPLA into stearic acid-doped lipid nanoparticles [22] or CpG into LNPs [18].

Combining adjuvants is an emerging strategy in the design of next-generation vaccine formulations. Single adjuvants often possess inherent limitations and are unable to elicit the entire repertoire of immune-stimulatory activities [23]. Consequently, multi-adjuvant formulations have gained attention as a promising approach to enhance vaccine efficacy [24]. Notably, GlaxoSmithKline (GSK) has pioneered the rational combination of adjuvants, exemplified by its use of classical adjuvants such as alum alongside novel TLR agonists [25].

To date, and to the best of our knowledge, no reports have described the use of LNPs as delivery platform for co-encapsulation of adjuvants targeting both intracellular and extracellular TLRs to achieve synergistic immune activation. Existing strategies have primarily focus in the administration of free TLRs agonists in vaccine formulations against complex diseases such as cancer, HIV, malaria and other infectious pathogens, as they help to shape adaptive immunity in a very precise manner [26]. In particular, the combination of free MPLA and CpG-ODNs has demonstrated potential to modulate transcriptional programs in innate immune cells, enhance DC function, and elicit broad-based immunity involving Th1, Th2, and antibody responses [27].

In this study, we demonstrate the feasibility of formulating LNPs with CpG-ODNs loaded in the aqueous core and MPLA integrated into the lipid shell. Structural characterization using small-angle X-ray scattering (SAXS) and cryogenic transmission electron microscopy (cryo-TEM) confirmed the integrity of the modified LNPs. The resulting LNP-MPLA-CpG formulation induced a strong innate immune response without compromising mRNA expression, underscoring its potential as a next-generation nanovaccine capable of eliciting sustained and robust immunity.

2. Materials and methods

2.1. Materials

CleanCap® Enhanced Green Fluorescent Protein (EGFP) mRNA and CleanCap® Firefly Luciferase (Luc) mRNA were obtained from TriLink BioTechnologies (San Diego, CA, USA). Monophosphoryl lipid A (MPLA) was sourced from InvivoGen (San Diego, CA, USA), and CpG-ODN 1826 was acquired from Miltenyi Biotec (Bergisch Gladbach, Germany). Lipids including ALC-0315 (((4-hydroxybutyl)azanediyl)bis(hexane-6,1-diyl)bis(2-hexyldecanoate)) and ALC-0159 (alpha-[2-(ditetradecylamino)-2-oxoethyl]-omega-methoxy-poly(oxy-1,2-ethanediyl)) were provided by Cayman Chemical (Ann Arbor, MI, USA). Additional lipids, such as DSPC and cholesterol, were obtained from Avanti Polar Lipids (Alabaster, AL, USA). PolyA was sourced from Merck KGaA (Darmstadt, Germany).

2.2. Synthesis of LNP formulations

LNPs were synthesized using a microfluidic system employing the NanoAssemblr® platform (Precision NanoSystems Inc., Vancouver, Canada) at a total flow rate of 12 ml/min, N/P ratio of 6 and a flow rate ratio (FRR) of 3:1 (aqueous to organic). The Initial and final waste volumes were 200 μl and 50 μl, respectively [28]. The self-assembly process involved combining a mRNA solution at 120 μg/ml in 50 mM citrate buffer at pH 4.0 with a lipid-containing ethanolic phase at 12.5 mM. The formulations derived from lipid mixtures (LM) with different compositions and aqueous phases (Aq.) with a reporter mRNA and CpG-ODN (or PolyA) at 5:1 ratio as it is listed in Table 1. After synthesis, LNPs were diluted in PBS at a ratio of 1:20 for *in vitro* experiments and at 1:40 for *in vivo* applications. Formulations were then up-concentrated using Amicon® centrifugal filters (50,000 MWCO) at 2000 ×g for 5 min per fraction to reach total mRNA concentrations in the range of 150–200 μg/ml. The resulting suspensions were sterile-filtered through a 0.22 μm membrane and stored at 4 °C for subsequent use.

Additionally, two preparation methods for further −80 °C long-term storage analysis were tested [29]. In cryo-method 1, after the synthesis of LNPs with the microfluidic technique, samples were diluted in cryo-preservation buffer composed of Tris 20 mM (pH 7.4), 150 mM NaCl and 10 % Sucrose (TBSS-buffer). Then, LNPs were processed as indicated before. In cryo-method 2, the final LNP formulations were dialyzed overnight from PBS to TBSS-buffer using Slide-A-Lyzer® MINI Dialysis Device, 10 K MWCO, 0.5 ml (Thermo Fisher Scientific Inc., Naarden, Netherlands).

For uptake experiments in DC2.4 cells, the LNPs composition was modified for visualization through fluorescent read-outs. The reporter EGFP mRNA was incorporated into the aqueous phase of the formulations. Additionally, the lipidic phase was modified through addition of the fluorescent labelled lipid DSPE-PEG(2000)-N-Cy5 at 0.1 mol% to the LM as a tracer of the nanoparticle uptake.

2.3. Determination of mRNA encapsulation efficiency (EE) by RiboGreen assay

mRNA was quantified using RiboGreen reagent (ThermoFisher, Waltham, MA, USA) by fluorescence detection at 535 nm (emission) after excitation at 485 nm. Measurements were conducted using a TECAN Spark® plate reader (Männedorf, Switzerland). The mRNA EE% was determined by measuring the mRNA concentration in LNP samples under two conditions: total mRNA content after incubation with 2 % Triton X-100 at 37 °C for 10 min and non-encapsulated mRNA without Triton X-100. Encapsulated mRNA was calculated from the difference between total mRNA content and the unencapsulated mRNA value.

2.4. Particle size, Zeta potential (Z-Pot), and polydispersity index (PDI)

The mean hydrodynamic diameter and polydispersity index (PDI) of the LNP samples were measured following a 1:100 dilution in PBS by dynamic light scattering (DLS) in a Nano ZS Zetasizer (Malvern Instruments Corp., Malvern, UK). The reported values for particle size are based on intensity-weighted measurements. *Z*-pot was measured with the same instrument using DTS1080 disposable capillary cells. The stability of the formulations was monitored weekly for up to one month by evaluating changes in particle size, Z-pot, and EE% during storage at 4 °C. Additionally, LNPs stability after storage at −80 °C was determined.

2.5. Cryogenic transmission electron microscopy (Cryo-TEM)

Size and morphology of LNPs were analyzed using the cryo-TEM technique in a TEM (FEI Titan Krios G4, Thermo Fisher Scientific, Naarden, The Netherlands) under cryogenic conditions. For this, samples were vitrified with a Vitrobot Mark V (ThermoFisher, Hillsboro, OR, USA) plunge freezing device. A volume of 3 μl of the sample dispersion was applied to a glow-discharged Quantifoil or lacey carbon-coated TEM grid (treated in an oxygen plasma cleaner, Diener Nano®, Diener electronic, Ebhausen, Germany). Excess solution was removed using filter paper, and the grid was immediately immersed in liquid ethane for vitrification. The samples were examined at an acceleration voltage of 300 kV using a 4 k Direct Electron Detection Camera (Gatan K3, Pleasanton, CA, USA) under low-dose conditions to preserve sample integrity. Micrographs were analyzed using ImageJ® software (version 1.54) [30].

2.6. Small-angle X-ray scattering (SAXS)

SAXS measurements were conducted at the NCD-SWEET beamline (Project ID 2023067620) of the ALBA Synchrotron Light Source in Barcelona, Spain. The experiment utilized an incident energy of 10 keV and a 3.2 m sample-to-detector distance. Samples were loaded into low-scattering polymeric capillaries (2.2 mm external diameter, 0.1 mm wall thickness). Data collection employed a Pilatus 1 M detector (Dectris, Switzerland), with azimuthal integration performed using the pyFAI library to obtain one-dimensional scattering profiles [31]. Scattering intensity was plotted against the momentum transfer q, defined as $q = \frac{4\pi}{\lambda} sin(\theta)$, where λ is the incident wavelength and 2θ the scattering angle. Each sample was measured in 10 frames of 10 s, discarding any affected by radiation damage. Experiments were conducted at 22 °C.

To investigate structural features, a polydisperse multi-shell spherical particle model was employed to represent the electron density variations in the outer layers of each product, as detailed in previous work [28]. In this approach, the scattering from a single particle is derived from contributions of its concentric shells, with the amplitude weighted by their respective volumes. The model was adapted from strategies used in neutron scattering studies of multi-shell particles [32]. Here, a bilayer nanoparticle featuring a homogeneous core was considered, with the core's radius following a Gaussian distribution (20 % standard deviation). The bilayer shell comprises two high-density polar regions and one low-density region, each with a fixed thickness of 2 nm. Additionally, a para-crystal structure factor was incorporated to describe the lamellar arrangement, with the set at 0.01. Under these conditions, the key fitting parameters were the mean core radius, the electron densities of the concentric shells, and the average number of

Table 1
Composition and characterization of the different mRNA-loaded LNP with the inclusion of adjuvants. The mean size, polydispersity Index (PDI), *Z*-potential (Z-pot), and mRNA-encapsulation efficiency (EE%) were determined.

Formulation	Composition								Characterization			
	Lipid Phase (Mol%) – 12.5 mM					Aqueous Phase (ratio) – 120 μg/ml			Size (nm)	PDI	Z-pot	EE%
	ALC 0315	DSPC	Chol	ALC 0159	MPLA	*Luc* mRNA	PolyA	CpG-ODN				
LNP	50.00	10.20	38.10	1.70	–	5	1	–	85.1 ± 0.2	0.08 ± 0.02	−5.5 ± 1.5	79.4 ± 7.0
LNP-CpG	50.00	10.20	38.10	1.70	–	5	–	1	79.4 ± 1.2	0.03 ± 0.01	−4.5 ± 2.6	84.1 ± 8.0
LNP-MPLA	49.75	9.95	37.85	1.45	1.0	5	1	–	84.1 ± 0.5	0.06 ± 0.02	−4.6 ± 0.5	90.7 ± 9.0
LNP-MPLA-CpG	49.75	9.95	37.85	1.45	1.0	5	–	1	86.2 ± 0.5	0.07 ± 0.03	−5.1 ± 0.3	86.0 ± 8.0

Abbreviations: Chol (Cholesterol); *Luc* (Luciferase); PolyA (Poly-Adenosines); ODN (oligodeoxynucleotides).

layers. Equations can be found in the previews published work [28].

2.7. Nanoparticle tracking analysis (NTA)

LNPs size and *Z*-Pot were also determined by NTA. Measurements were obtained in a ZetaView PMX-230 Twin Laser (Particle Metrix, Mebane, NC, USA), following previous indication for optimal NTA analysis [33]. LNPs were also live monitored with a high-resolution camera to check the presence of aggregates and the degree of homogeneity.

2.8. Determination of LNPs pKa

The apparent pKa of nanoparticles was measured by the 6-(p-toluidino)-2-naphthalenesulfonic acid sodium salt (TNS) fluorescence method [34]. Cayman's LipidLaunch™ LNP Apparent pKa Assay Kit/TNS Method was used in the determination of pKa of LNPs. TNS exhibits fluorescence when interacting with positively charged membranes, allowing for easy quantification in a plate reader (TECAN Spark® plate reader (Männedorf, Switzerland) at $\lambda_{ex} = 320$ nm and $\lambda_{em} = 450$ nm. As TNS dissociates, its fluorescence decreases. Consequently, titrating the pH in the presence of LNPs generates a curve, with the point at which fluorescence reaches 50 % of its maximum defined as the apparent pKa of the particle. The measurements and calculations were performed according to manufacturer's instructions.

2.9. Evaluation of in vitro mRNA expression levels

To evaluate the ability of LNP formulations to deliver and effectively express the encapsulated reporter mRNA, transfection experiments were performed in different DCs types. Mouse DCs (DC2.4) and human monocyte-derived DCs (MoDCs) were selected as cellular models of DCs from mice or human origin. Luciferase expression was measured following previous protocols with the Promega Luciferase Assay kit (WI, USA), according to manufacturer's recommendations in a TECAN Spark® plate reader (Männedorf, Switzerland), equipped with an automatic injector.

2.9.1. DC2.4 cell line transfection

DC2.4 cells were cultured in RPMI-1640 medium supplemented with 10 % iFBS, 1 % antibiotics (100 U/ml penicillin and 100 μg/ml streptomycin), 1 % L-glutamine (2 mM), 1× non-essential amino acids, 1 mM HEPES, and 0.0054× β-mercaptoethanol. Cells were seeded in 96-well plates at a density of 1.5. $\times 10^4$ cells per well for 24 h. LNP formulations at mRNA concentration of 0.67 μg/ml and 6.67 μg/ml per well, respectively, were used for transfection over a 24 h period. A 30 μl aliquot of supernatant was collected from each well and stored at −20 °C for subsequent cytokine analysis [35].

2.9.2. MoDCs transfection

Monocytes were isolated from human peripheral blood mononuclear cells (hPBMCs) obtained from at least five healthy donors using the CD14 MicroBeads Human MACS kit (Miltenyi Biotec Bergisch Gladbach, Germany) following the manufacturer's protocol. Briefly, hPBMCs were counted and a total number of 4.5×10^8 cells was pelleted by centrifugation. The cell pellets were resuspended in 80 μl of MACS buffer and 20 μl of CD14 MicroBeads per 10^7 cells were added. After a 15 min incubation at 4 °C, the cells were washed with MACS buffer and subsequently resuspended in 500 μl of MACS buffer per 10^8 cells.

The cell suspension was applied to a LS column (Miltenyi Biotec) placed in a magnetic field and the column was washed three times with MACS buffer to remove unbound cells. Finally, the column was mechanically flushed with MACS buffer to elute the CD14-positive monocytes. The eluate was centrifuged, and the resulting cell pellet was resuspended in MoDCs medium (RPMI1640, 10 % FBS, 1 % L-Glutamine). The monocyte cell suspension was then counted, and 3×10^6 cells were seeded in 3 ml in each well on a 6-well plate with MoDCs culture medium supplemented with the granulocyte-macrophage colony-stimulating factor (GM-CSF) at a concentration of 100 ng/ml for differentiation to MoDCs and, IL-4 at a concentration of 25 ng/ml to prevent concomitant macrophage differentiation. Following a 48 h incubation at 37 °C, half of the culture medium was replaced with new MoDCs fresh culture medium containing IL-4 (50 ng/ml) and GM-CSF (200 ng/ml). After an additional 72 h incubation, cells were seeded as required in a 96-well plate and used for transfection.

2.10. Cellular uptake and expression kinetics

The kinetics of uptake and expression of LNPs by DCs (2.4 cell line) were studied at different exposition times. For transfection 2.5×10^4 cells per well were seeded in a 48-well plate and transfected with 0.67 μg/ml of EGFP mRNA loaded into fluorescent LNPs (Cy5 labelled). Kinetic measurements, after 3, 6 and 24 h were performed. Cells were washed twice with PBS and consequently the fluorescence intensity of Cy5 was measured using a TECAN Spark® plate reader (Männedorf, Switzerland) ($\lambda_{ex} = 620$ nm and $\lambda_{em} = 680$ nm). EGFP expression and the Cy5 signal in the cells were also analyzed by fluorescent microscopy on an Olympus CKX41 instrument (Tokyo, Japan). Afterwards, PBS supernatant was discarded, and cells were detached by trypsinization. Following a 5 min of incubation at 37 °C, cells were resuspended in FACS buffer (1× PBS with 2 % iFBS), transferred to a 96-v bottom plate and centrifuged (400 ×*g*, 5 min). The supernatant was discarded by inversion and cells were resuspended in 200 μl of FACS buffer. Flow cytometry data were acquired using a FACSymphony™ A3 (Becton, Dickinson and Company, Franklin Lakes, NJ) and analyzed using FlowJo™ software version 10.8 (Ashland, OR, USA; Becton, Dickinson and Company).

2.11. Cryopreservation study

The suitability of different cryo-preservation buffers to facilitate long-term storage at −80 °C of mRNA-loaded LNPs was studied. Therefore, DC2.4 cells were transfected with LNPs directly prepared in TBSS buffer (cryo-method 1) or dialyzed from PBS to TBSS (cryo-method 2). Transfection efficiency was measured by fluorescence microscopy and flow cytometry after 7 and 28 days of cryopreservation. The physicochemical properties of cryopreserved LNPs were also determined in terms of size and PDI by DLS, and EE by RiboGreen.

2.12. Cytokines and chemokines quantification

Cell culture supernatants or serum samples were collected after LNP treatment. The levels of TNF-α, IFN-γ and IL-2 (primarily associated with Th1-cells); IL-4 and IL-10 (associated with Th2-cells); IL-6 and IL-17 A (associated with Th17-cells) were measured using multiplex Cytometric Bead Array (CBA). For MoDCs supernatants, the LEGENDplex™ HU Essential Immune Response Panel was used, while for DC2.4 cell supernatants, the LEGENDplex™ MU Th Cytokine Panel was employed (BioLegend, San Diego, CA, USA). The release of IL-12p70 was specifically measured in MoDCs. Samples were acquired using a FACSymphony™ A3 (BD) and data were analyzed with the LEGENDplex™ data analysis software version 8.0 at https://legendplex.qognit.com/workflow.

2.13. Hemotoxicity studies

Heparinized venous blood from healthy donors was collected with written informed consent from the Institute of Transfusion Medicine of the University Medical Center, Mainz. Whole blood was placed in a 12-well culture plate containing Hanks´ balanced salt solution (HBSS) in a 1:100 ratio and transfected with 0.67 μg/ml of each LNP formulation at 37 °C for 1 h. After incubation, the blood–LNP suspension was centrifuged at 2500 ×*g*, 37 °C for 5 min, and the resulting precipitate was

discarded. The extent of red blood cell lysis was quantified by measuring the released hemoglobin at $\lambda_{max} = 540$ nm. Hemolysis was defined as 100 % by exposing erythrocytes to 1.0 % Triton X-100 and PBS incubation as negative control [36].

2.14. Cellular viability by MTT assay

To measure cellular proliferation and viability, a colorimetric assay based on MTT ((3-(4,5-Dimethylthiazol-2-YI)-2,5-Diphenyltetrazolium Bromide)) was performed according to manufacturer's protocol (Roche, "Cell Proliferation Kit I (MTT): Colorimetric assay for the non-radioactive quantification of cell proliferation and viability" Cat. No. 11465 007001). 2×10^4 DC2.4 cells were seeded in a 96-well plate with 100 µl of culture medium per well and incubated for 24 h at 37 °C with 5 % CO_2. After incubation, 50 µl of supernatant was carefully removed, and cells were treated with either LNP (0.67 µg/ml), EtOH (positive control, C^+), or culture medium alone (negative control, C^-). Culture medium was then added to bring the final volume to 100 µl per well. Following incubation, 10 µl of MTT reagent (final concentration 0.5 mg/ml) was added to each well, and plates were incubated for an additional 4 h. Next, 100 µl of solubilization solution was added. Plates were incubated overnight at 37 °C with 5 % CO_2, after which absorbance at 570 nm was measured using a TECAN Spark® plate reader (Männedorf, Switzerland).

2.15. In vivo mRNA expression and cytokine release after LNP administration

Three groups of mice (each $n = 5$; BALB/cAnNCrl) were intramuscularly (i.m.) injected with 50 µl of the following: (i) PBS, (ii) 5 µg of *Luc* mRNA/LNP and (iii) 5 µg of *Luc* mRNA/LNP-MPLA-CpG, respectively. After 5.30 h, submandibular blood was collected, and serum was isolated for cytokine analysis. For the biodistribution experiment, at 6 h timepoint luciferin was intraperitoneally (i.p.) administered, and the mice were anesthetized with isoflurane mixed with oxygen. Luciferase expression was monitored by bioluminescence in an IVIS Spectrum CT instrument (PerkinElmer, USA) and exposure of 0.5, 1, 3 or 5 s were recorded. Cervical dislocation was used for euthanasia and organs, including the heart, lungs, liver, kidneys, spleen, auxiliary lymph nodes and muscle, were dissected and imaged. For quantification liver and spleen were weighed. Images were analyzed using Living Image Software (PerkinElmer, USA).

2.16. Splenocytes and liver non-parenchymal cells (NPCs)

Spleens were mechanically disrupted using a pestle and a cell strainer (40 µM; Greiner Bio-One, Frickenhausen, Germany). Spleen cells (4×10^6/ml) were cultured in IMDM-based media supplemented with 2 mM L-glutamine, 100 U/ml penicillin, 100 µg/ml streptomycin (all from Sigma-Aldrich), 50 µM ß-mercaptoethanol (Roth), and 5 % FBS (PAN-Biotech, Aidenbach, Germany). To isolate liver NPCs, livers were subjected to enzymatic dissociation (Liver Dissociation Kit; Miltenyi Biotec, Bergisch-Gladbach, Germany) as recommended by the manufacturer. Liver tissue was cut into small pieces that were transferred into prepared C tubes (Miltenyi Biotec) and minced in a gentle MACS Dissociator (program m_liver_03). The obtained cell suspension was incubated under continuous shaking (30 min at 37 °C), followed by another dissociation step (m_liver_04). Liver NPCs were enriched by density centrifugation (30 % Histodenz-HBSS; Sigma-Aldrich) and resuspended (10^6/ml) in RPMI 1640-based media containing 10 % FBS (PAN Biotech), 50 µM ß-mercaptoethanol (Roth), 1 % L-L-glutamine, 1 % non-essential amino acids, 100 U/ml penicillin, 100 µg/ml streptomycin, 10 mM HEPES, 1 mM sodium pyruvate (all from Sigma-Aldrich). Spleen cells and liver NPCs were seeded into sterile round –bottom polystyrene tubes (each 500 µl) and differentially treated as indicated. The next day, supernatants were retrieved for subsequent cytokine detection and cells were assayed by flow cytometric analysis using an Attune NxT Flow Cytometer (Thermo Scientific), equipped with Attune NxT software (ThermoScientific).

2.17. Statistical analysis

A one-way ANOVA followed by Fisher's LSD test was employed to compare groups. For comparisons involving multiple variables, a two-way ANOVA was applied. The *p*-values were interpreted as follows: $p < 0.05$ (*), $p < 0.01$ (**), $p < 0.001$ (***), and $p < 0.0001$ (****) were considered statistically significant. Non-significant differences were labelled as "ns".

3. Results

3.1. LNP formulation design

To study the effect of incorporating CpG-ODN and MPLA adjuvants into the structure of LNPs, different combinations of organic and aqueous phases were investigated (Table 1).

LNPs were generated using a microfluidic platform by combining the lipid phase (LM) and aqueous phases (Aq.) as presented in Table 1: LNP (ALC-0315/DSPC/cholesterol/ALC-0159) + (*Luc* mRNA + PolyA (at 5:1 ratio)); LNP-CpG: (ALC-0315/DSPC/cholesterol/ALC-0159) + (*Luc* mRNA + CpG-ODN at (5:1 ratio); LNP-MPLA: (ALC-0315/DSPC/cholesterol/ALC-0159/MPLA 1 %) + (*Luc* mRNA + PolyA in (5:1 ratio); and LNP-MPLA-CpG: (ALC-0315/DSPC/cholesterol/ALC-0159/MPLA 1 %) + (*Luc* mRNA + CpG-ODN in (5:1 ratio)). Formulations were developed by incorporation of CpG into the aqueous phase of the LNPs, while MPLA was included into the lipidic phase due to their respective hydrophilic and lipophilic characteristics (Fig. 1).

Physicochemical characterization of LNPs demonstrates their integrity after adjuvant incorporation.

Size, polydispersity, *Z*-pot and EE% were relevant parameters to determine the stability of the developed formulations, as well as the effect on the properties after incorporation of each adjuvant into LNPs. These physicochemical characteristics are crucial for assessing the quality and potential efficacy of LNP-based vaccine formulations (Table 1 and Fig. 2).

The intensity-weighted size values of LNPs were in the range of 85 to 90 nm. Incorporation of CpG, MPLA and the combination of both resulted in LNPs with a similar mean size (Fig. 2a). The PDI of all formulations was lower than 0.1, suggesting the presence of highly monodispersed nanoparticles (Fig. 2b). Size and PDI are important factors influencing the biodistribution, pharmacokinetic and cellular uptake of LNPs. Typically, LNPs with a size range of 50–200 nm and a PDI below 0.3 are considered optimal for vaccine delivery [37]. The *Z*-pot of all formulations was close to neutrality, with values in the range of 0 to −8 mV (Fig. 2c). Furthermore, the presence of adjuvants did not significantly affect the surface charge of LNPs ($p>0.05$). The EE is another critical parameter that determines the amount of mRNA successfully incorporated into LNPs. All developed formulations showed EEs higher than 85 % (Fig. 2d).

To confirm the stability of LNPs formulations over time, their physicochemical properties in terms of mean size, PDI, Z-pot and EE were monitored at regular intervals over 28 days of storage at 4 °C. The results showed that LNPs, with or without adjuvants, maintained consistent size, stable Z-pot and low PDI throughout the study period, indicating robust structural integrity and uniform particle size distribution.

To further investigate the structural properties of LNPs after adjuvant incorporation, cryo-TEM measurements were complemented by SAXS analysis (Fig. 2 e-f). Cryo-TEM images revealed consistent LNP sizes of all formulations with a mean diameter of approximately 40–60 nm, in agreement with previous observations [38] (Fig. 2e). TEM and other microscopic techniques provided a direct visualization of the

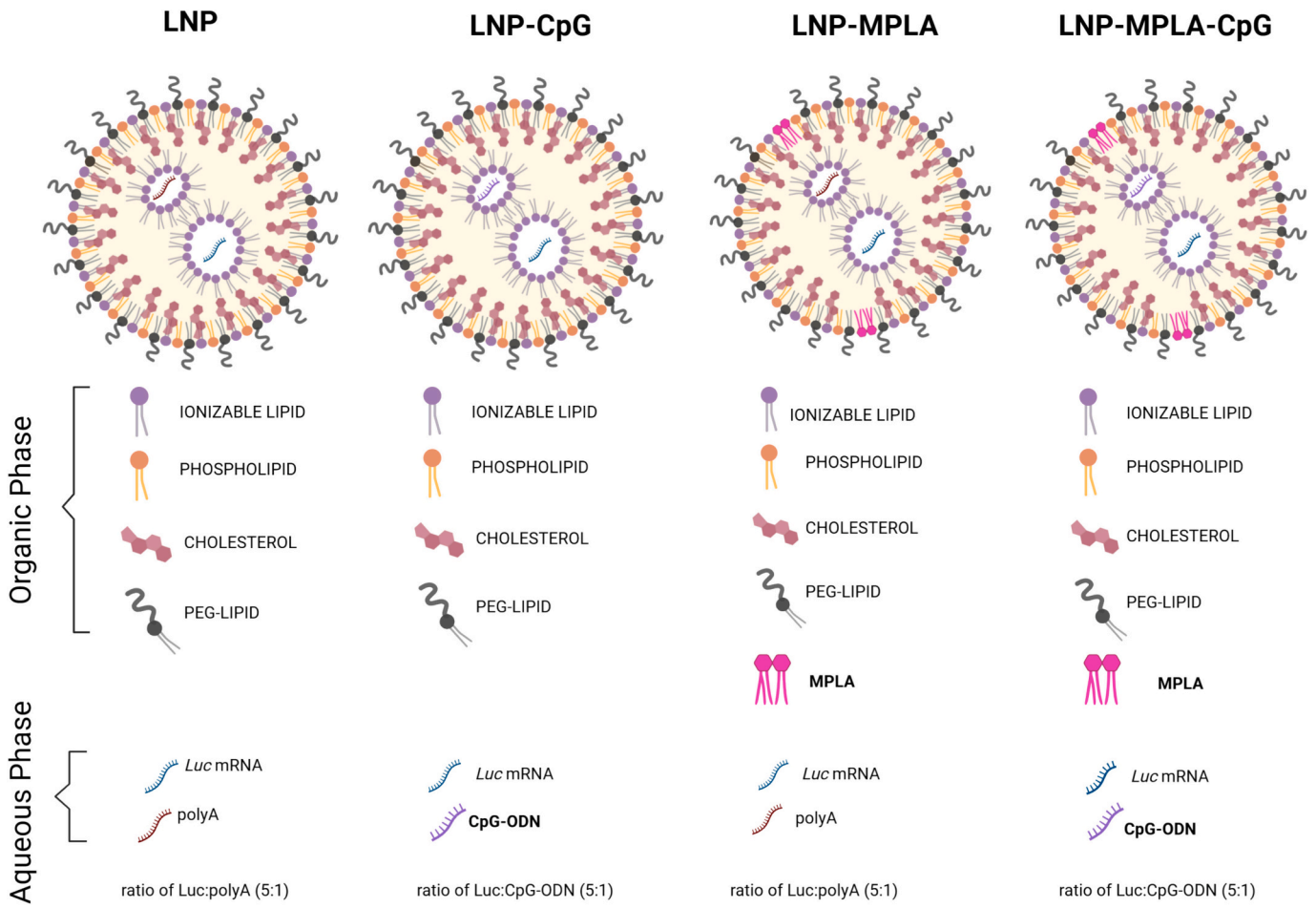

Fig. 1. Schematic design and composition of different LNPs with the theoretical structural incorporation of adjuvants (Created in BioRender. Meyer, C. (2025) https://BioRender.com/z00n558). CpG-ODN was included in the aqueous phase of LNPs, while MPLA was incorporated in the lipid mixture during LNPs preparation. *Luc* mRNA was used as reporter, while polyA as an inert RNA-like sequence.

nanoparticle core in a dehydrated state. This discrepancy in size with DLS is also observed after determination of the core size with SAXS (Fig. 2f).

Deeper morphology observations also allowed the detection of "bleb" structures in the LNP formulations containing MPLA, CpG and both adjuvants (Fig. 2e and Fig. S1). A similar architecture was observed in control LNP without adjuvants, suggesting that the inclusion of these adjuvants has minimal impact on the typical structural properties of LNPs Such two-compartment structures are frequently observed in LNPs encapsulating mRNAs or other large nucleic acids [39]. As seen across all images, the nanoparticles were predominantly spherical, exhibiting homogeneous size and shape.

SAXS studies revealed the presence of characteristic concentric structures of LNPs (Fig. 2f). According to the SAXS patterns, the presence of spherical nanoparticles with potentially bilamellar structures could be elucidated, showing a distinctive broad peak near 1 nm^{-1}. Based on previous studies, the pattern could be related to nanoparticles size as well as lipid stacking [35]. The mean nanoparticle size could also be estimated from the small-angle region. All formulations displayed a polydispersity around 15 %, which could be decreased by considering the presence of smearing effects or surface LNP defects into the model. While LNPs showed a mean particle size around 67.4 nm, LNP-CpG, LNP-MPLA and LNP-MPLA-CpG exhibited diameters around 66.4, 74.0 and 72.8 nm, respectively. This slight increase in LNP size after MPLA inclusion suggests the effective inclusion of the lipopolysaccharide analogue into the LNP architecture.

Additionally, the mean size and *Z*-pot of LNP and LNP-MPLA-CpG formulations were determined by NTA (Fig. 3a-b). LNP showed a narrow peak around 91.7 nm, whereas LNP-MPLA-CpG exhibited a mean size around 87.8 nm, consistent with the values obtained by DLS. Z-pot for both formulations were − 13.1 and − 9.2 mV respectively, suggesting the presence of slightly negative nanoparticles. Furthermore, live monitoring images of LNPs revealed the presence of well dispersed nanoparticles without the presence of aggregates and a high degree of homogeneity.

The apparent pKa of LNPs was determined before and after the incorporation of both adjuvants (Fig. 3c). After titration in the presence of the fluorescent dye 6-(p-toluidino)-2-naphthalenesulfonic acid across a range of pH, the pKa values were determined to be 6.5 for LNP and 6.4 for LNP-MPLA-CpG. These values fall within the expected range for conventional LNPs and represent a critical parameter, as the pKa significantly influences endosomal escape and, consequently, the efficiency of cellular transfection [34].

3.2. *LNPs containing adjuvants maintain high mRNA translation levels in human and mouse DCs*

The *Luc* mRNA expression levels in murine DC2.4 cell line and human MoDCs were evaluated using a luciferase assay detection method (Fig. 4 a-b). Maintenance of protein expression levels is crucial for the efficient delivery of mRNA to target cells and tissues [40]. MoDCs were used as a primary human immunological model. All examined immune cell types were transfected with an mRNA concentration of 0.67 μg/ml. Higher mRNA concentrations of 6.67 μg/ml did not result in increased

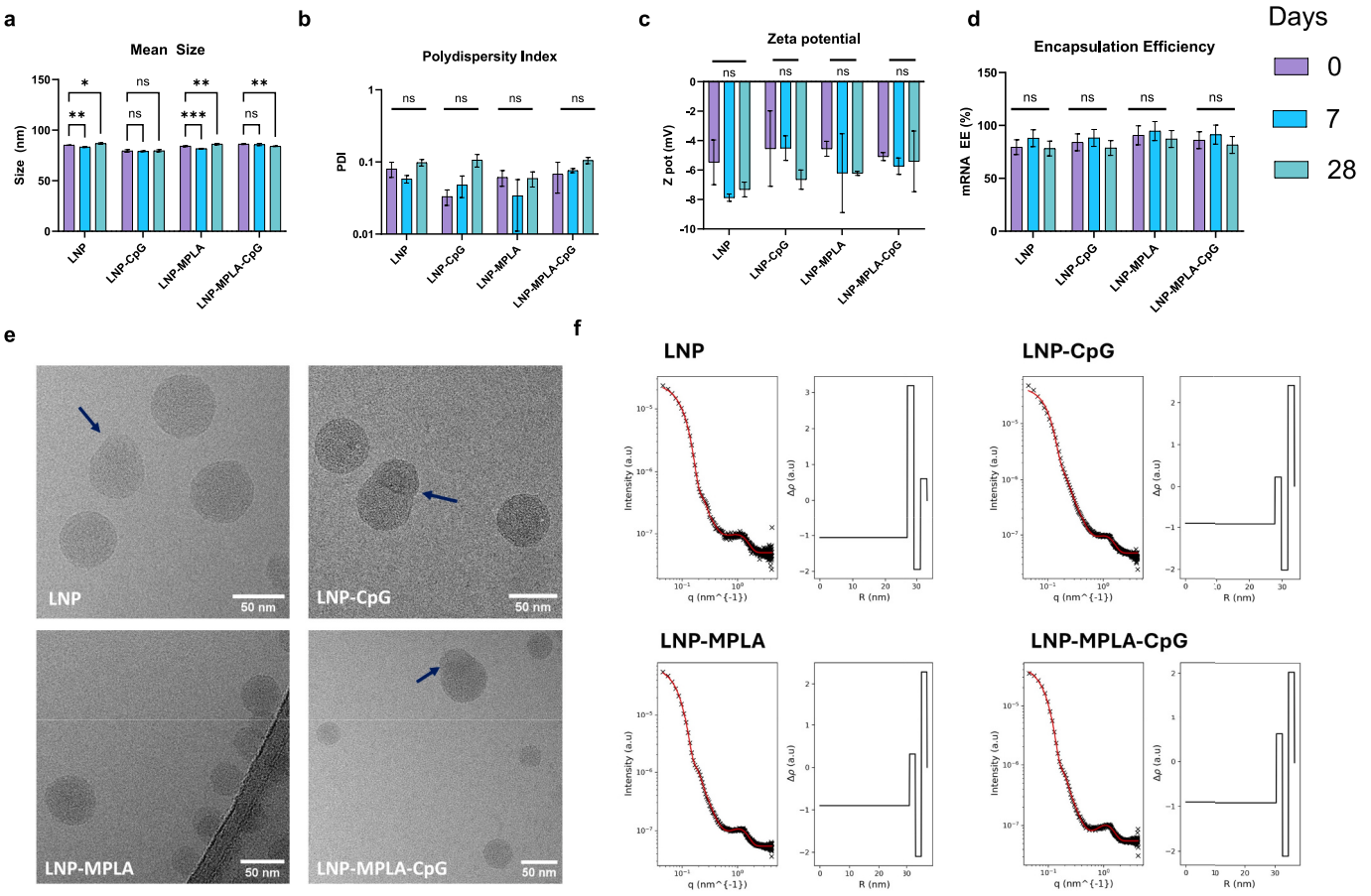

Fig. 2. Physicochemical properties and stability assays of LNP formulations after storage at 4 °C. Mean size (a), polydispersity index (PDI) (b) and Z-pot (c) were measured by DLS. The encapsulation efficiency (d) was determined by RiboGreen assay. Those parameters were followed at 4 °C for 1 month. The graphs represent the mean ($n = 3$) ± SD. Four different LNP formulations were observed by Cryo-TEM (e). The presence of bleb structures in LNP is indicated with dark blue arrows. Size analysis and figures were created with ImageJ. SAXS profiles of LNPs were also acquired (f). The left graph shows the Log plot of the experimental SAXS pattern and the fitted curve in continuous line. The right column shows the electron density profile obtained from the bilayer mode. Two-way ANOVA followed by Fisher's LSD test was used to compare between groups: $p < 0.05$ (*), $p < 0.01$ (**), $p < 0.001$ (***) and ns (not significant; $p > 0.05$).

mRNA expression (Fig. S2). Therefore, subsequent experiments were conducted using an mRNA concentration of 0.67 μg/ml. After 24 h incubation with the LNP formulations, the levels of released cytokines in the supernatants were measured (Fig. 4 c-d).

The luciferase expression levels ranged from 1.0×10^6 to 1.0×10^7 luminescence units for all tested formulations in DC2.4 (Fig. 4a). No significant reduction in mRNA expression was observed for DC2.4 cells transfected with LNP-MPLA or the dual-adjuvant formulation LNP-MPLA-CpG. The LNP and LNP-CpG formulations exerted low levels of cytokine expression after transfection of DCs (Fig. 4c). In contrast, formulations containing MPLA, and particularly the combined MPLA and CpG co-delivery, yielded significantly higher levels of pro-inflammatory cytokine expression. Notably, TNF-α levels were increased by 65-fold and 155-fold in the case of LNP-MPLA and LNP-MPLA-CpG, respectively, compared to LNP. A similar tendency was observed for IL-6, with cytokine expressions rising by 85-fold and 479-fold, respectively, in response to treatment with LNP-MPLA and LNP-MPLA-CpG. Additionally, the effects of free adjuvants on cytokine release were evaluated in DC2.4 cells. The levels induced by free adjuvants were comparable in magnitude to those observed with the encapsulated adjuvants (Fig. S3).

Analysis of MoDCs revealed no significant inhibition of reporter protein expression following treatment with LNP-encapsulated adjuvants (Fig. 4b). Although luciferase expression levels in these primary cultures were between 3 and 4 orders of magnitude lower than those observed in the DC2.4 cell line, both cell types exhibited significant expression levels. Treatment with LNP-CpG resulted in low cytokine release (Fig. 4d). However, consistent with findings in DC2.4 cells, the inclusion of MPLA induced robust secretion of TNF-α and IL-10, cytokines associated with a Th1 and Th2 response, respectively. Additionally, elevated levels of IL-6 were also observed, suggesting a potential role in promoting a Th17 response. Notably, the LNP-mediated co-delivery of MPLA with CpG led to a two-fold increase in TNF-α and IL-10 levels. This finding demonstrated the synergistic benefits of incorporating multiple adjuvants (MPLA and CpG) into the LNP architecture, resulting in an enhanced immune response. Given the critical role of the IL-12 cytokine family in cell-mediated immunity, levels of the pro-inflammatory cytokine IL-12p70 were measured in MoDCs treated with the different LNP formulations. While LNP and LNP-CpG did not induce IL-12p70 release, LNP-MPLA triggered the secretion of approximately 1180 pg/ml of IL-12p70. Importantly, the combinatory formulation LNP-MPLA-CpG, further increased cytokine levels to 2445 pg/ml representing a twofold increase and suggesting an enhanced immune response likely to promote Th1 cell differentiation.

3.3. LNPs are taken-up by DCs in a time dependent manner

DCs play a crucial role in bridging innate and adaptive immune responses. To evaluate the ability of DCs to phagocytize LNPs, Cy5-labelled DSPE was incorporated into the lipid phase of the LNPs. In parallel, the aqueous phase was adjusted by replacing the reporter *Luc*

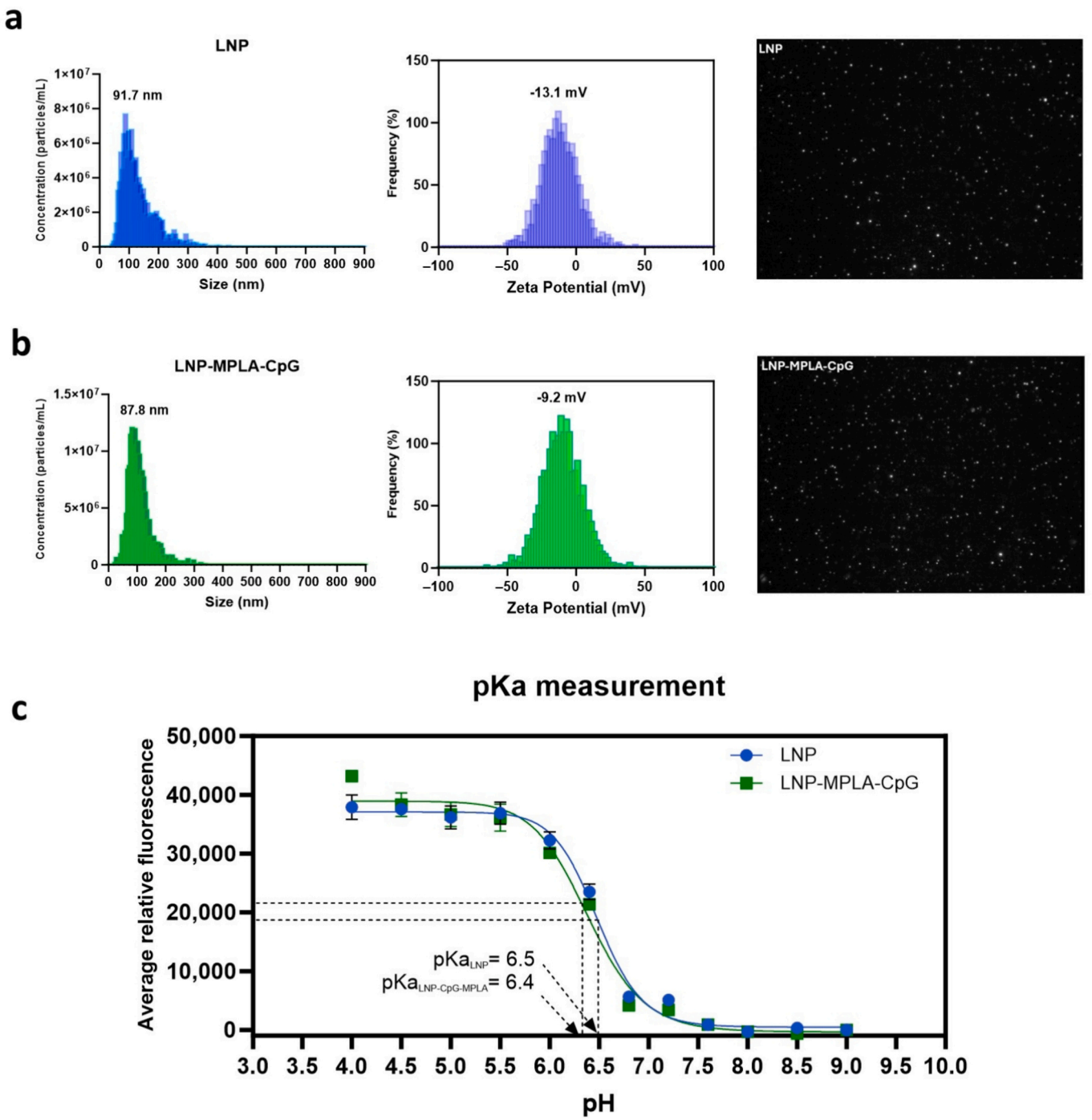

Fig. 3. Size and Z-pot distribution of LNP (a) and LNP-MPLA-CpG (b) by NTA. Live monitoring of LNPs was conducted to assess the presence of aggregates and the degree of homogeneity. The pKa of those formulations was determined with the Cayman's LipidLaunch™ LNP Apparent pKa Assay Kit/TNS method (c).

mRNA with *EGFP*-encoding mRNA. A time-course experiment was conducted to monitor LNP uptake by assessing Cy5 fluorescence intensity as well as the expression of the EGFP protein, providing insights into cellular internalization and transfection efficiency, respectively (Fig. 5).

Both kinetics were monitored by fluorescence microscopy (Fig. 5a). Images illustrate EGFP and Cy5 signal after 0, 3, 6 and 24 h of transfection. As the brightfield images depicts, healthy rounded cells with consistent morphology across all conditions were observed. Although fluorescence signals were low at the earlier time points (0, 3 and 6 h), overlapping images at 24 h showed that the same cells that internalized LNPs, as indicated by the red Cy5 signal, also expressed EGFP, confirming successful mRNA delivery. Notably, LNP-MPLA-CpG showed slightly lower EGFP expression and Cy5 signal compared to LNP alone. Complementary, the fluorescent Cy5 signal due to LNP internalization was followed by fluorescent spectroscopy, indicating a Cy5 signal increase over time for both formulations, peaking at 24 h. These results confirm efficient uptake and intracellular processing of LNPs by DCs, even in the presence of co-encapsulated adjuvants.

The LNP uptake and reporter expression time kinetic results obtained were also confirmed by flow cytometric analysis (Fig. 5b). The gating analysis of the events acquired demonstrated the gradual migration of the DC population toward positive signals for both Cy5 and EGFP over time, suggesting simultaneous LNP internalization and mRNA

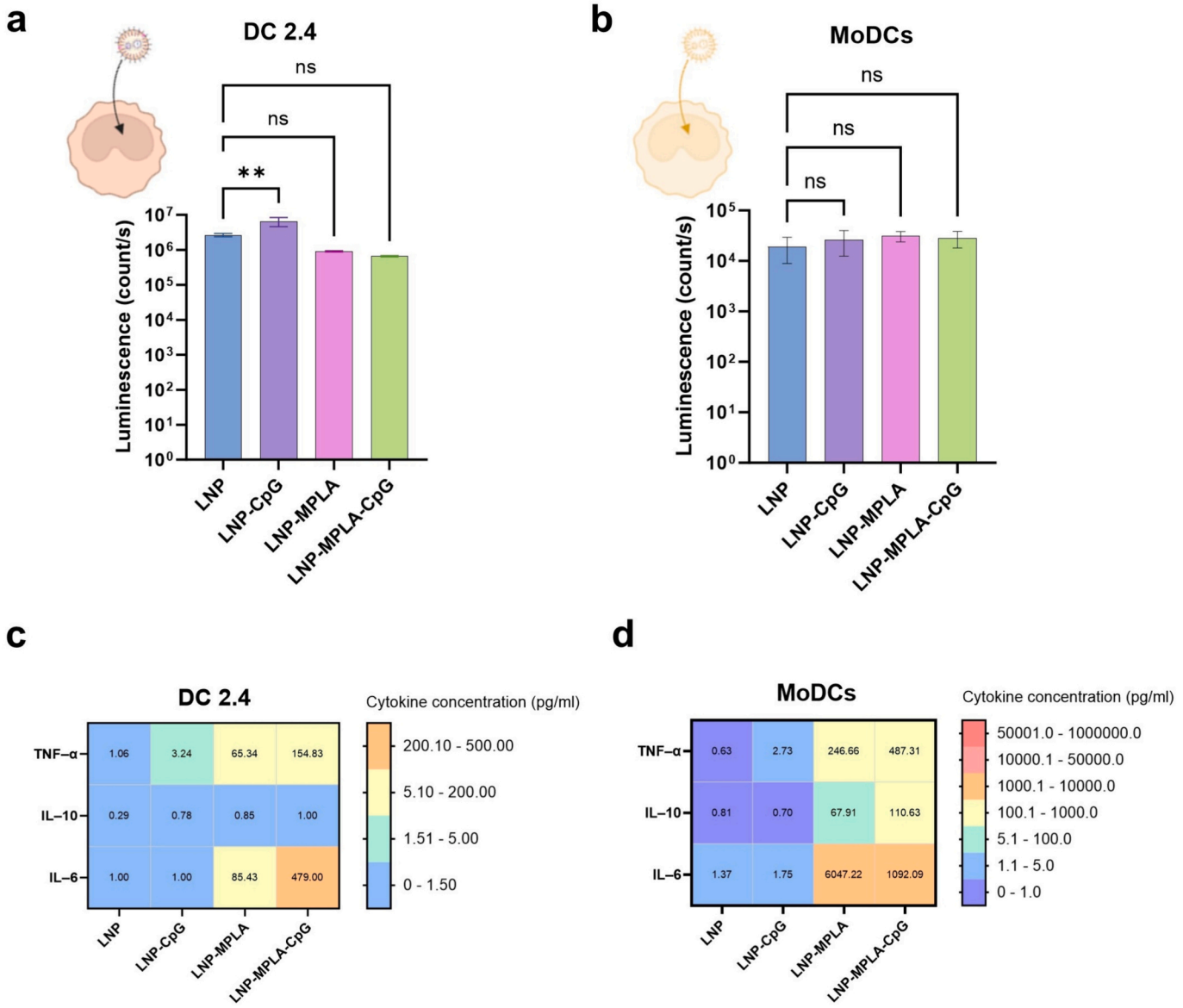

Fig. 4. Evaluation of Luc mRNA expression and cytokine secretion after LNP transfection in different models of DC types. Transfection of DC2.4 cells (a) and human MoDCs (b) with LNPs at 0.67 μg/ml of mRNA was performed. Luciferase measurements were made after 24 h of transfection. The graphs represent the mean $n = 4$ (MoDCs) ± SD; and mean $n = 3$ (DC2.4) ± SD. One-way ANOVA followed by Fisher's LSD test was used to compare between groups: $p < 0.05$ (*), $p < 0.01$ (**), $p < 0.0001$ (****) and ns (not significant; $p > 0.05$). Cytokine secretion produced after 24 h of transfection was determined in DC2.4 cells (c) and MoDCs (d) by cytometric bead assay. The graphs represent the mean ($n = 5$) of the most representative cytokines for each cell line.

expression. After 24 h, up to 100 % of DCs had internalized the LNPs and expressed the EGFP protein. Overall, LNP-MPLA-CpG exhibited a similar nanoparticle uptake rate as LNP but demonstrated lower EGFP transfection efficiency.

3.4. LNPs are stable after cryopreservation at −80 °C upon dialysis method

To determine optimal cryopreservation conditions for long-term storage of LNPs, various preparation methods were evaluated (Fig. 6). In cryo-method 1, LNPs were dialyzed from PBS to TBSS (Fig. 6a). No significant changes in the physicochemical properties of cryopreserved LNPs were observed in terms of size and PDI by DLS, as well as EE by RiboGreen (Fig. 6b). Transfection efficiencies in DC2.4 cell line confirmed that the method was reliable in maintaining mRNA stability after 7 and 28 days of storage. Furthermore, cellular internalization, as indicated by Cy5 fluorescence, remained unchanged, supporting the stability of LNP uptake properties post-cryopreservation (Fig. 6c).

Cryo-method 2 involved a process in which LNPs were directly diluted in TBSS buffer immediately after synthesis (Fig. 6a). Although this method resulted in changes to the physicochemical properties of LNPs following cryopreservation, both mRNA transfection efficiency and LNP cellular internalization properties were maintained (Fig. 6b-c). Larger nanoparticles were observed for both LNP and LNP-MPLA-CpG formulations upon testing cryopreservation method 2, with mean sizes around 150 nm and elevated PDI values, indicating reduced colloidal stability. Despite these changes, the EE remained unaffected. The observed increase in particle size and PDI suggests the presence of aggregates in the formulation, which could compromise the proper delivery of LNPs to target organs such as the spleen, essential for eliciting an effective immune response [41]. Consequently, cryo-method 1 was selected for all subsequent experiments.

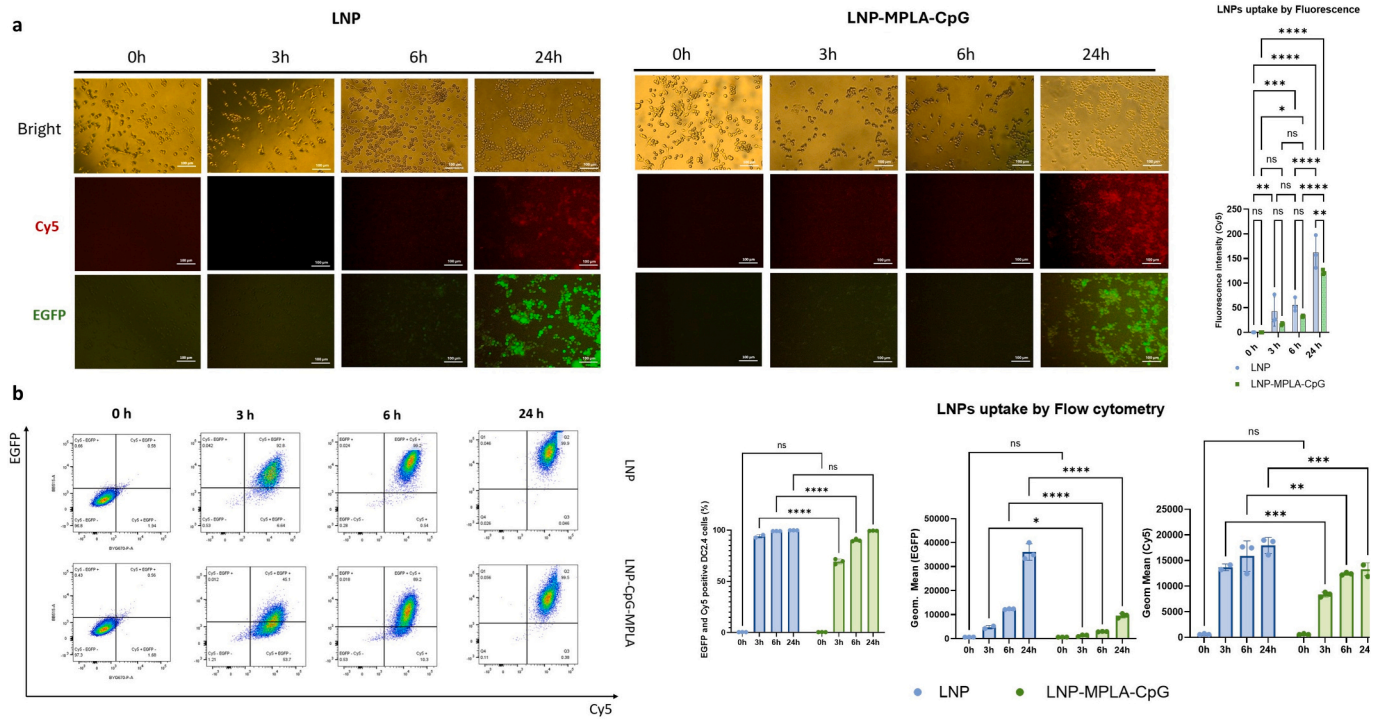

Fig. 5. Cellular uptake of LNP and LNP-MPLA-CpG by DC2.4. Fluorescence microscopy of time-course analysis of LNPs uptake after 0, 3, 6 and 24 h of transfection. The uptake of Cy5-labelled LNPs was followed by fluorescence spectroscopy (a). Complementary, the percentage of EGFP and Cy5 positive cells was detected using flow cytometry at 0, 3, 6 and 24 h after transfection (b). Geometric mean of EGFP and Cy5 signal was calculated with FlowJo™ software version 10.8 (Ashland, OR, USA; BD). Two-way ANOVA followed by Fisher's LSD test was used to compare between groups: $p < 0.05$ (*), $p < 0.01$ (**), $p < 0.001$ (***), $p < 0.0001$ (****) and ns (not significant; $p > 0.05$).

3.5. LNPs with encapsulated adjuvants demonstrate biocompatible properties

Efficient translation of mRNA delivered by adjuvant-encapsulated LNPs is a critical factor to determine vaccine efficacy. Therefore, evaluating the biocompatibility of these formulations is essential for future clinical applications and for initial studies in animal models [42]. Prior to conducting *in vivo* experiments, mouse and human cells were exposed to LNP formulations in order to assess their biocompatibility *in vitro* (Fig. 7a).

Cell viability of DC2.4 cells following transfection with LNP formulations was assessed using 7-AAD staining and analyzed *via* flow cytometry (Fig. 7b). The data showed no significant reduction in cell viability across any LNP-treated group compared to untreated controls ($p > 0.05$), indicating that the LNP formulations did not induce notable cytotoxicity. Although a slight decrease in viability was observed, the adjuvants administered in a soluble form did not exert a statistically significant reduction in cell viability (Fig. S4a). However, treatment with of DC2.4 cell line with free CpG or free MPLA led to a marked reduction in cell viability (about 40 %) highlighting the potential cytotoxic effects of unencapsulated adjuvants. This finding suggests that LNPs provide a safe deliver mode for adjuvants to target cell populations. These results were further corroborated by metabolic assay, which confirmed that DC viability remained above 80 % following treatment with all LNP formulations (Fig. 7c).

Hemotoxicity was assessed after exposing whole blood samples to different LNPs and adjuvant combinations for 1 h (Fig. 7d). According to the ISO/TR 7406 standard, biomaterials which less than 5 % hemolysis are considered safe for biomedical applications [43]. LNPs with encapsulated adjuvants induced minimal hemotoxicity (LNP- CpG, LNP-MPLA and LNP-MPLA-CpG). This is relevant considering that free adjuvants such as MPLA and its combinations displayed significant hemolysis levels close to 5 % (Fig. S4b). This suggests that adjuvants formulated into LNPs exert fewer toxic effects compared to non-encapsulated adjuvants.

3.6. In vivo biodistribution

Biodistribution of LNPs containing the indicated adjuvants was studied in naïve BALB/c mice following i.m. administration of 5 μg of encapsulated *Luc* mRNA (Fig. 8a).

Blood samples were collected within the first 6 h after injection and serum was isolated to measure cytokine release induced by LNPs (Fig. 8b). Cytokine measurements in blood serum revealed a strong stimulation by the LNP-MPLA-CpG formulation after i.m. injection, mainly of cytokines associated with a Th1-response. IFN-γ levels increased more than 300-fold, accompanied by a remarkable 15-fold increase in TNF-α, compared to the PBS group. Only a 10-fold increase in IL-6 levels was observed. In contrast, LNP treatment alone did not resulted in a significant increase in those cytokines levels.

Whole-body bioluminescence was measured and quantified to assess *in vivo* antigen expression (Fig. 8c). Compared to the LNP group, the LNP-MPLA-CpG formulation exhibited lower Luc expression at both the injection site and in the liver ($p < 0.05$). Nevertheless, the bioluminescence signal remained strong (greater than 10^7 radiance units) indicating effective antigen expression capable of eliciting a potential immune response. Interestingly, organ-specific biodistribution imaging illustrated that LNPs co-encapsulating adjuvants distributed primarily in the liver, spleen, lymph nodes and, importantly, at the injection site in the muscle (Fig. 8d).

3.7. Stimulation of splenocytes and NPCs with LNP/adjuvants triggers DC immune activation and cytokine release

In light of the biodistribution results, showing predominant accumulation of LNPs in the spleen and liver, immunomodulatory effects on

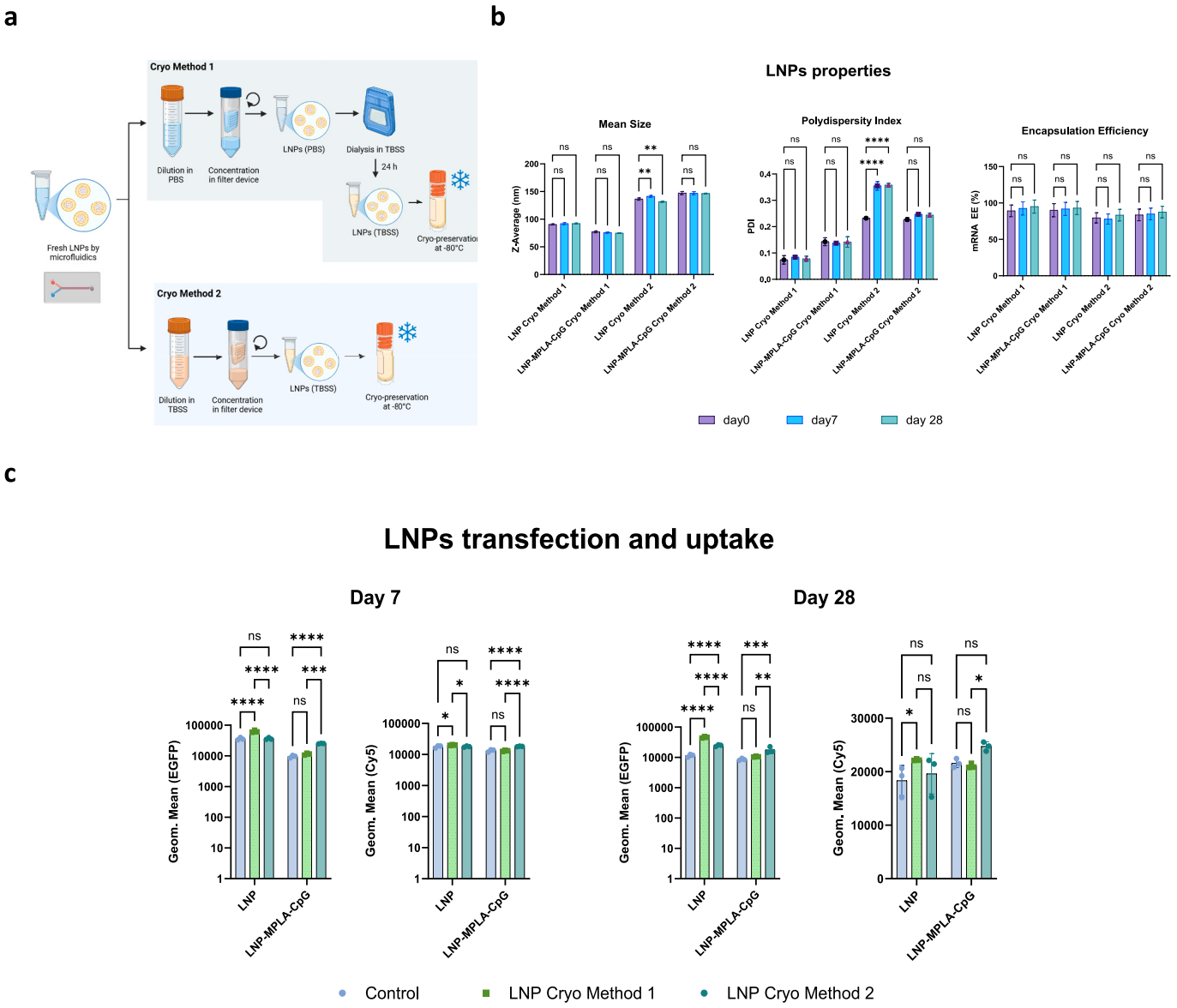

Fig. 6. Physicochemical properties and stability assay of Cy5 labelled and *EGFP* mRNA encapsulated LNP formulations after cryopreservation at −80 °C. (a) Schematic representation of two methods for LNPs preparation, which involved the dialysis from PBS to TBSS (Cryo Method 1) or the dilution of LNPs in TBSS buffer (Cryo Method 2) (Created in BioRender. Islan, G. (2025) https://BioRender.com/p4a9b8o). (b) The mean size, polydispersity index (PDI) and mRNA encapsulation efficiency were followed at −80 °C for 1 month under the two cryopreservation conditions. (c) DC2.4 cells were transfected with cryopreserved LNPs following the previously mentioned protocol and transfection efficiency as well as LNP uptake was measured *via* flow cytometry after 7 and 28 days of cryopreservation. The graphs represent the mean ($n = 3$) ± SD. Two-way ANOVA followed by Fisher's LSD test was used to compare between groups: $p < 0.05$ (*), $p < 0.01$ (**), $p < 0.001$ (***), $p < 0.0001$ (****) and ns (not significant; $p > 0.05$).

corresponding cell populations (splenocytes and liver NPCs) were further examined *in vitro*. Splenocytes and liver NPCs were harvested and *in vitro* incubated with the respective LNP formulations for 24 h to assess their immune activation potential (Figs. 9 and 10).

Expression of activation markers on different cell subtypes from spleen was evaluated (Fig. 9b). In conventional DCs (cDCs 1 and 2), treatment with adjuvant-containing LNPs led to increase expression levels of the co-stimulatory molecules CD80 and CD86 of 1.5-fold and 2-fold, respectively, compared to non-transfected control cells. While plain LNP did not elicit a significant increase in these markers, the inclusion of CpG, MPLA, or their combination induced a clear activation of both cDC subsets. Meanwhile, plasmacytoid DCs (pDCs) elicited only a slight activation on the expression of CD80 and CD86 in response to the formulations. Notably, in the case of PMN, the LNP-MPLA-CpG induced an increase of 2 and 1.5 times the expression of CD80 and CD86, respectively (Fig. S5).

Stimulation of splenocytes with adjuvant loaded-LNPs triggered the release of various cytokines (Fig. 9c). The potential of the LNP formulations to induce cytokine and chemokine release associated with Th1, Th2, and Th17 immune responses was investigated. Interestingly, LNP-CpG induced a robust stimulation, leading to a significant increase in cytokines associated with a potential Th1-type response, including IFN-γ, TNF-α, IP-10, and CCL5. In particular, IFN-γ levels showed a remarkable 46-fold increase compared to the control LNP. In contrast, LNP-MPLA induced a more moderate response, with a 10-fold increase in cytokine secretion. However, the combination of both CpG and MPLA into the LNP demonstrated a potent effect, leading to a 162-fold increase in IFN-γ. Additionally, LNP-CpG induced the release of cytokines and chemokines associated with a Th2-type response. In that case, IL-10 and CCL2 levels increased, reaching approximately 300 pg/ml. Evidence of a

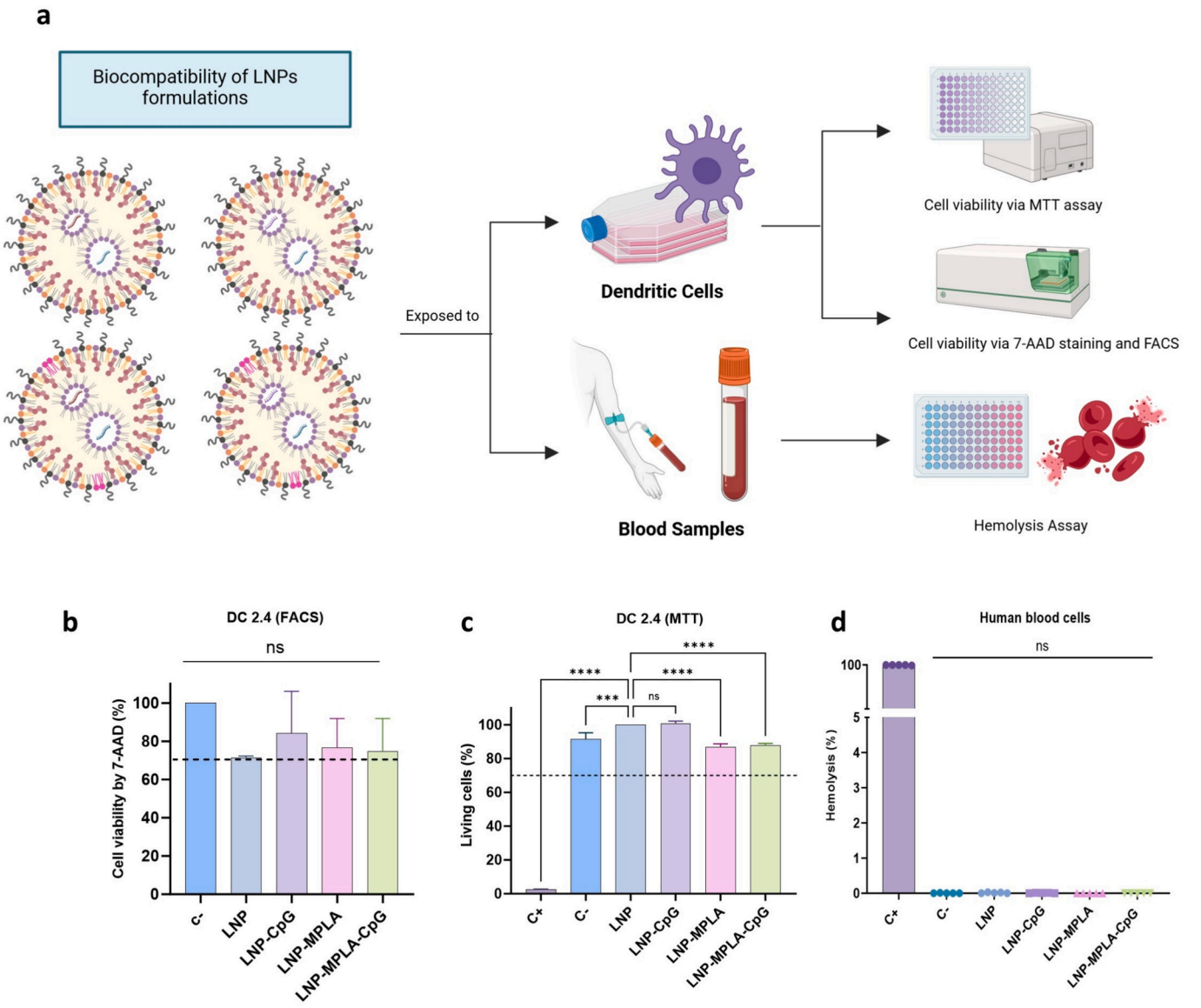

Fig. 7. Biocompatibility assays of LNP formulations were conducted as follows: (a) scheme of read-outs for biocompatibility analysis of LNPs which were performed (Created in BioRender. Islan, G. (2025) https://BioRender.com/zcg5aok); (b) cytotoxicity in the mouse DC2.4 cell line by flow cytometry and (c) MTT assay. (d) Hemolytic activity in whole blood samples after 1 h of exposure to the different LNP formulations. The results express the mean ± SD ($n = 3$). One-way ANOVA followed by Fisher's LSD test was used to compare between groups: $p < 0.001$ (***), $p < 0.0001$ (****) and ns (not significant; $p > 0.05$).

potential Th17 response was also observed following LNP-CpG stimulation, characterized by a moderate increase in IL-1β and CXCL1, along with a pronounced release of IL-6. For MPLA-loaded LNPs, the elevated secretion of IP-10 and CCL5, along with a moderate increase in TNF-α, suggested the induction of a Th1-type response. However, the concurrent presence of substantial levels of IL-10, CCL2, and IL-6 also indicated possible involvement of Th2 and Th17 pathways. The LNP formulation containing both MPLA and CpG elicited a combined cytokine profile, integrating the effects observed with the individual adjuvant-loaded LNPs.

Since most of the LNPs reached the liver after i.m. administration, the immunological response in NPCs was also assessed [44] (Fig. 10a). NPCs comprise a complex immune cell population, including Kupffer cells (KC), liver sinusoidal endothelial cells (LSECs) and DCs. Within the DCs population, only the LNP-MPLA-CpG formulation induced a significant increase of CD80 and CD86 ($p < 0.05$) cell surface expression markers (Fig. 10b). A similar trend was observed in the case of KC for CD80 (Fig. S6). In KCs and LSECs, an upregulation of CD86 was observed following treatment with LNP-CpG, LNP-MPLA and LNP-MPLA-CpG. LNP treatment did not induce a significant increase in that cell activation marker ($p > 0.05$).

Cytokine release in LNP-stimulated NPCs was also evaluated (Fig. 10c). LNP-CpG induced robust secretion of IFN-γ, IFN-α, and IFN-β, along with moderate levels of other cytokines such as TNF-α, IP-10, and CCL5. This cytokine profile is consistent with a strong immune activation capable of promoting a Th1-type response. A similar profile was observed for LNP-MPLA formulation, which elicited the release of IFN-γ, TNF-α and IFN-β at levels between 7 and 60-fold higher than those induced by LNP. Additionally, a moderate increase in the levels of Th2-related cytokines IL-10 and CCL2, as well as Th17-associated cytokines/chemokines including IL-1β, GM-CSF, IL-6, and CXCL1, was observed. Although no synergistic effects were observed by LNP-MPLA-CpG treatment, the cytokine secretion levels remained elevated compared to control LNPs without adjuvant.

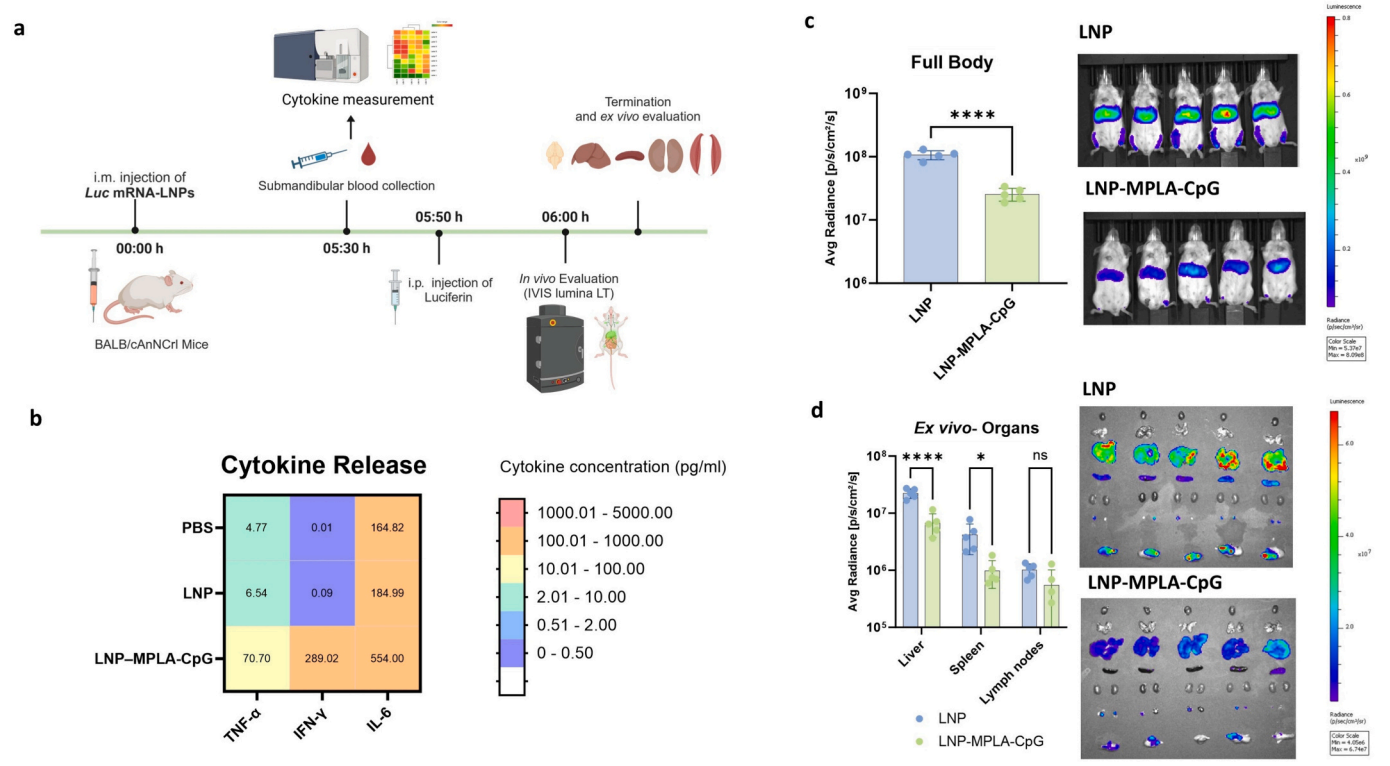

Fig. 8. *In vivo* biodistribution and cytokine release of LNPs determined in a naïve BALB/c mouse after i.m. injection of 5 μg of *Luc* mRNA and LNPs with or without adjuvants as indicated. (a) Scheme of the experimental approach and the respective bioluminescence read-outs (Created in BioRender. Islan, G. (2025) https://BioRender.com/z42fvsw). (b) Blood samples were collected within the first 6 h after injection and serum was isolated to measure cytokine release induced by LNPs. (c-d) Exposure time was 0.5 s for full body and organ images (from top to bottom: heart, lungs, liver, spleen, kidneys, lymph nodes and muscle). Graphs represent the mean of the region of interest (ROI) ($n = 5$) ± SD. One-way or two-way ANOVA followed by Fisher's LSD test were used to compare between the groups. $p < 0.05$ (*), $p < 0.0001$ (****) and ns: not significant ($p > 0.05$).

4. Discussion

While LNP-mRNA vaccines are capable of eliciting antigen-specific immune responses, they often fail to induce robust and long-lasting immunity. To improve their efficacy and better tailor the immune response, combining LNPs with additional adjuvants has emerged as a promising strategy [5]. Adjuvants such as CpG (a TLR9 agonist) and MPLA (a TLR4 agonist) help direct and strengthen adaptive immunity, particularly in the context of therapeutic vaccines aimed to combating chronic or dificult-to-eradicate infections [18,20,26,45]. The dual-adjuvant formulation, LNP-MPLA-CpG, demonstrated promising outcomes in terms of immunostimulation, mRNA translation, and biocompatibility. A key strength of this study lies in the systematic, side-by-side comparison of all four formulations (LNP, LNP-MPLA, LNP-CpG, and LNP-MPLA-CpG), which enabled the direct attribution of specific immunological and physicochemical effects to each adjuvant. Incorporating adjuvants into the LNP structure enhanced their innate immune activation. While LNP-CpG did not elicit significant *in vitro* innate stimulation in DCs or MoDCs, MPLA induced a robust Th1-associated cytokine response. However, stimulation of splenocytes and NPCs with LNP-CpG resulted in elevated cytokine secretion, suggesting a potential Th1-skewed immune response. The combination of both adjuvants may ensure effective immune activation in diverse cellular types, particularly in immunologically tolerogenic environments, as observed with NPC stimulation. This comparative approach revealed the distinct and synergistic contributions of MPLA and CpG to DC activation and cytokine production.

To the best of our knowledge, this is the first time MPLA and CpG have been successfully encapsulated into mRNA-delivering LNPs, demonstrating excellent stability, homogeneity, and high EE. The formulation strategy resulted in the inclusion of CpG into the aqueous phase of LNPs, while MPLA was integrated into the lipid architecture. The combination of two adjuvants demonstrated enhanced effects on immune cells, presumably through concomitant stimulation of the intracellular TLR 9 (CpG) and the extracellular TLR 4 (MPLA). Both CpG-ODN and MPLA are adjuvants approved for *in vivo* applications and are already used in clinical trials, particularly in several licensed vaccines [13,17].

A recent study developed a non-mRNA influenza vaccine by delivering the hemagglutinin H5 antigen alongside CpG and MPLA using a squalene-based nanoemulsion (AddaVax) [46]. The combination of both adjuvants enhanced vaccine efficacy, leading to increased levels of homologous and cross-reactive IgG, as well as hemagglutination-inhibiting antibodies against influenza virus [47]. However, these approaches did not include the co-encapsulation of both adjutants into LNPs.

In our study, lipid mixtures were optimized based on previous studies from our laboratory [28,35]. The N/P ratio (positive charge on cationic lipid to negative charge on CpG/mRNA) was maintained at 6, intended for i.m. route of administration [37]. The LNP-MPLA-CpG nanoparticles showed desirable size and PDI for development of vaccines, which are important factors influencing the biodistribution and cellular uptake of LNPs. Typically, LNPs with a size range of 50–200 nm and a PDI below 0.3 are considered optimal for vaccine delivery [37]. Further, the production of LNPs with near-neutral *Z*-pots is often desirable to enhance cellular uptake while minimizing non-specific interactions [48]. High encapsulation values are essential for optimizing the delivery of mRNA to target cells and tissues [40].

Cryo-TEM images revealed consistent LNP sizes for all formulations, displaying a mean diameter of about 40–60 nm in line with literature [38]. The low diameter in comparison with DLS values is attributed to the fact that DLS measures the hydrodynamic radius of nanoparticles, which includes the solvation layers of water [49]. TEM and other

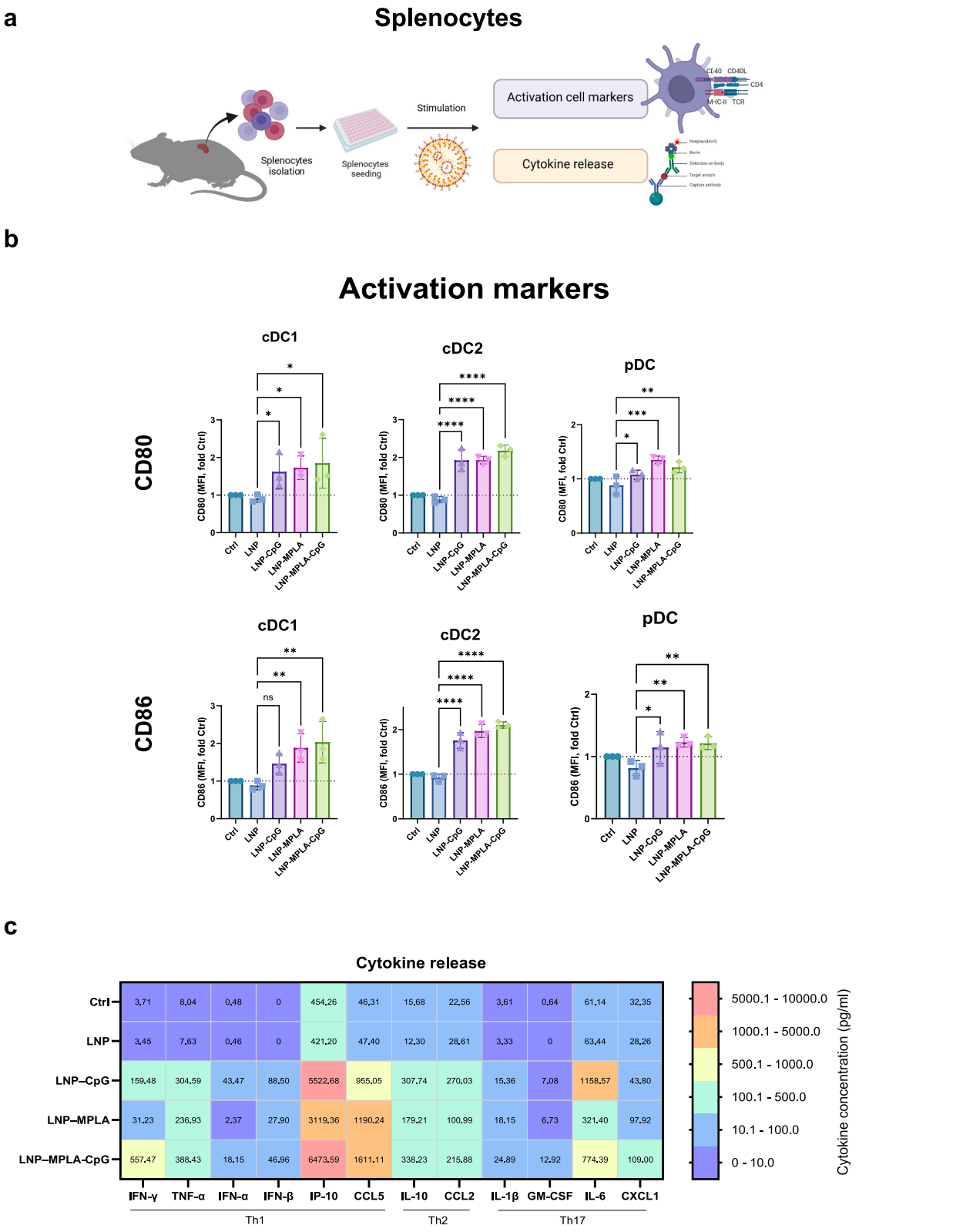

Fig. 9. Expression of activation markers in different cell subtypes and cytokine release after stimulation of splenocytes with different LNP/adjuvant formulations (a) (Created in BioRender. Islan, G. (2025) https://BioRender.com/nsks9bi). Cultures were treated overnight with LNP containing 1 μg/ml of mRNA; cells treated with R848 (1 μg/ml) served as positive controls. CD80 and CD86 were evaluated by flow cytometry (b). Cytokines in the supernatant of splenocyte cultures were quantified with cytometric bead arrays (c). Data are the means ± SEM ($n = 3$). One-way ANOVA followed by Fisher's LSD test were used to compare between the groups. $p < 0.05$ (*), $p < 0.01$ (**), $p < 0.001$ (***), $p < 0.0001$ (****) and ns: not significant (p >0.05). Abbreviations: cDC1/2: conventional dendritic cell subtype 1 and 2, pDC: plasmacytoid DCs.

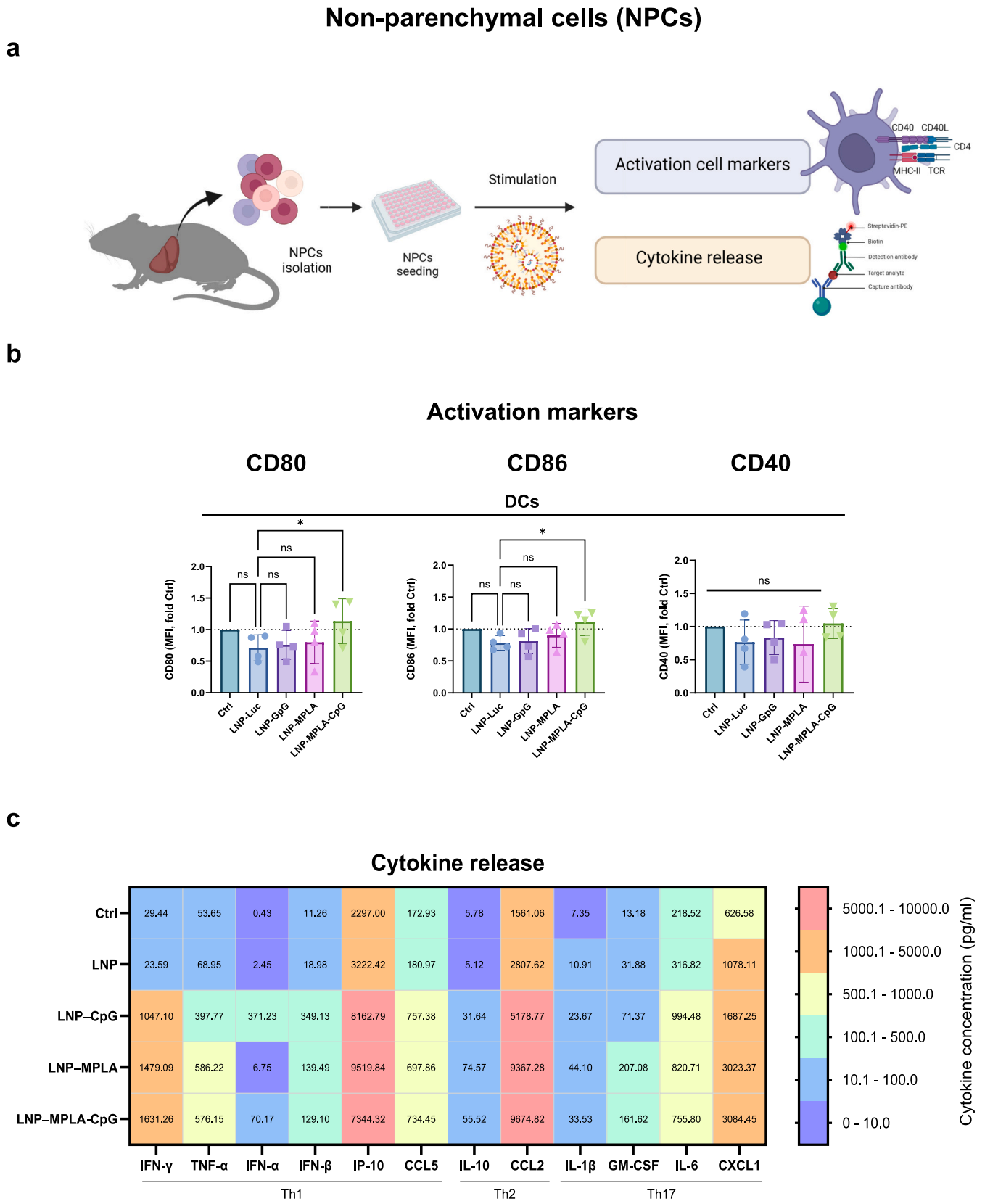

Fig. 10. Modulation in the expression of activation markers in different cell subtypes and the release of cytokines after stimulation of non-parenchymal cells (NPCs) with different LNP/adjuvant formulations (a) (Created in BioRender. Islan, G. (2025) https://BioRender.com/nsks9bi). Cultures were treated overnight with LNPs containing 1 μg/ml of mRNA; cells treated with R848 (1 μg/ml) served as positive controls. CD80, CD86 and CD40 were evaluated by flow cytometry (b). Cytokines in the supernatant of NPCs cultures were quantified with cytometric bead arrays (c). Data are the means ± SEM ($n = 3$). One-way ANOVA followed by Fisher's LSD test were used to compare between the groups. $p < 0.05$ (*), $p < 0.01$ (**) and ns: not significant ($p > 0.05$).

microscopic techniques provide a direct visualization of the nanoparticle core in a dehydrated state. This discrepancy in size was also observed after determination of the crystallographic core with SAXS. According to the SAXS patterns, the presence of spherical nanoparticles with potentially bilamellar structures could be confirmed. Based on previous studies, the pattern could be related with nanoparticles size as well as lipid stacking [35]. While LNPs showed a mean crystal size around 67.4 nm, LNP-CpG, LNP-MPLA and LNP-MPLA-CpG exhibited diameters around 66.4, 74.0 and 72.8 nm, respectively. This slight increase in LNP size after MPLA inclusion suggests the effective inclusion of the lipopolysaccharide analogue into the LNP architecture. The developed LNPs exhibited two-compartment structures which are frequently found in LNPs encapsulated with mRNAs or other large nucleic acids [39]. In addition to that, the presence of bleb structures in LNPs has been shown to be related with improved *in vivo* transfections. Consequently, the observation of bleb structures especially in the dual-adjuvant formulation is a promising sign for further cellular and *in vivo* expression assays [50].

The pKa is another critical parameter to characterize LNPs, as it influences their ability to efficiently transfect cells [34]. Here the pKa values were determined to be 6.5 for LNP and 6.4 for LNP-MPLA-CpG. Those values fall within the range of conventional LNPs and represent a critical parameter, as pKa influences the efficiency of cellular transfection [34].

Determining the optimal storage conditions for mRNA-LNPs remains an important but underexplored area, critical for maintaining the long-term stability and functional integrity of the formulations [29]. To evaluate the optimal cryopreservation parameters, two different freezing methods were tested. It was concluded that LNPs remain stable after cryopreservation at −80 °C using the dialysis method. Direct dilution of LNPs into the cryo-buffer led to the formation of aggregates within the formulation, which could compromise the efficient mRNA delivery to target organs such as the spleen, essential for mounting an effective immune response [41].

The mRNA expression levels of luciferase were high in MoDCs and DC2.4 cells after transfection with LNP-MPLA-CpG. High protein expression levels are crucial in the delivery of mRNA to target cells and tissues [40]. It has been reported that in the presence of certain MPLA levels, mRNA-mediated luciferase protein expression decreases but subsequently returns to normal levels, indicating an intrinsic balance between immune response modulation and protein expression by mRNA constructs [22].

LNP formulation is highly dependent on the therapeutic target of the delivered mRNA, either harnessing or mitigating innate immune responses is required. For instance, in vaccinations, maintaining a certain level of immunostimulatory activity is necessary, whereas in protein replacement therapies, the priority is to achieve of high and sustained protein expression while minimizing immune activation [51]. Notably, the development of new mRNA vaccines involving LNP engineering requires a delicate balance between activating innate immune responses and mitigating excessive responses to optimize protein expression [52,53].

DCs play a crucial role in bridging innate and adaptive immune responses. The ability of immature DCs to phagocytize LNPs was assessed by incorporating Cy5-labelled DSPE into the lipid phase of the LNPs. Flow cytometric gating analysis demonstrated the migration of the DC population over time toward positive signals for both Cy5 and EGFP, suggesting subsequent LNP internalization and mRNA expression respectively. After 24 h, up to 100 % of DCs internalized the LNPs and expressed the EGFP protein. Overall, LNP-MPLA-CpG exhibited a similar nanoparticle uptake rate as LNP but demonstrated lower EGFP expression efficiency.

The cytokine profile induced by LNP-mediated adjuvant delivery in DCs, primarily revealed an enhanced Th1 immune response, particularly as elicited with LNPs co-delivering both MPLA and CpG adjuvants. This combination represents a promising strategy for inducing protective immunity against certain infectious diseases [54]. Those results also demonstrated the synergistic benefits of incorporating distinct and complementary adjuvants into the LNP architecture to enhance the immune response. Pro-inflammatory cytokines, especially TNF-α and IL-6, play an important role in the activation of the innate immune system, which is essential for initiating adaptive immunity and controlling bacterial and viral infections [55,56]. The high expression levels of TNF-α, IFN-γ are characteristic of a Th1 dominated immune response [57]. This is in agreement with other works reporting that *OVA* mRNA LNPs/boosted adjuvant activity by inducing Th1 immune responses through the activation of multiple TLRs following intravenous injection [22]. Similarly, CpG-ODN encapsulation into LNPs has shown to increase levels of IFN-γ and inducing a Th1-biased immune response [58]. This Th1-biased immune polarization is particularly relevant for efficient immune responses against intracellular pathogens. Furthermore, the presence of IL-6 suggested a potential contribution to a Th17 response [59]. In the case of MoDCs, an enhanced production of the IL-12p70 after LNP-MPLA-CpG stimulation was observed. This cytokine, a member of the IL-12 family, is a key factor in promoting the immune response toward a clinically beneficial Th1-type pro-inflammatory immunity. Muller-Berghaus et al., reported the importance of IL-12p70 secreted from MoDCs in response to bacterial and viral components [60]. Additionally, Carreno et al., highlighted the critical role of IL-12p70 production in improved clinical outcomes among melanoma patients, emphasizing the therapeutic relevance of this cytokine in DC-based vaccines [61].

An efficient mRNA expression of LNPs with encapsulated adjuvants is a critical factor for their potential use in vaccine development. Furthermore, assessing the biocompatibility of these formulations is essential for future *in vivo* studies and consequently for their clinical application [42]. It the present study it was observed that LNPs provide a safe vehicle for delivering adjuvants to cells and even reduce toxicity when compared to the non-encapsulated adjuvants. *In vitro* results showed cell viability higher than 80 % in all LNP formulations. Our results align well with previous reports showing that nanoencapsulation of different compounds reduced their intrinsic cytotoxicity [62]. According to the ISO/TR 7406 standard, biomaterials exhibiting less than 5 % hemolysis are considered safe for biomedical applications [43]. Our LNPs co-encapsulating two adjuvants showed minimal hemotoxicity, thereby meeting this safety criterion.

The *in vivo* biodistribution results are in line with other studies, where LNP containing *Luc* mRNA, showed bioluminescence signals primarily in the liver, followed by spleen and lymph nodes [35,63]. Targeting the spleen and lymph nodes has emerged as a crucial strategy for developing optimal vaccine responses. The observed biodistribution provides the characteristics for efficient vaccination strategies [64]. In contrast with *in vitro* experiments, the LNP-MPLA-CpG formulation exhibited lower Luc expression at the injection site and in the liver compared to the LNP group. However, this fact does not represent a limitation for effective vaccine development. In other work from our laboratory, the production of antibodies against the OVA-target was not affected by the co-application of LNPs with different adjuvants, despite a reduction in *OVA* mRNA expression was observed. The translated OVA levels were, nevertheless, enough to mount a humoral response similar to that observed for OVA-LNPs alone [5].

Besides lymph nodes the spleen is one of the secondary lymphoid organs of preference to initiate and shape an antigen-specific immune responses. Its diverse pool of immunological cell populations, including T and B lymphocytes, macrophages, and DCs, provides a suitable *in vitro* model for evaluating the effects of LNPs containing adjuvants on immune cell activation. The cellular immune response induced by LNP-MPLA-CpG was specifically *in vitro* tested in cells derived from spleen, as the critical target organ for successful immunizations [22]. An effective up-regulation of CD80 and CD86 activation markers of conventional and plasmacytoid DCs in presence of LNP-MPLA-CpG was significantly observed. Activation of cDCs is the base of the so-called

"cancer immunity cycle" driven by their ability to activate T-cells [65]. Stimulation of pDCs, on the other hand, and particularly through TLR9, induces the secretion of type I interferons, key cytokine that eradicates viral and bacterial infections [65,66]. pDCs influence T cell response by promoting their activation and polarization toward a Th1 immunity, in conjunction with the induction of cytokine release by cDCs. For instance, studies in mice have shown that cDCs stimulated with CpG produce interleukins to combat Listeria infection, only when they have been previously activated by pDCs [66]. Notably, the observed cytokine profile trigged by LNP-MPLA-CpG included elevated secretion of IFN-γ and TNF-α as well as in the chemokines CXCL1 and IP-10 by splenocytes, which indicates a robust Th1 like immune response [57]. Our results support the concept that combining adjuvants within an LNP can enhance the immune response [47]. In addition, the increase in IL-10 indicates an enhancement of Th2 responses.

Given that most LNPs primarily target the liver, understanding the immune response within this environment becomes an important and necessary area to explore [67]. NPCs are mainly composed of Kupffer cells (KC), liver sinusoidal endothelial cells (LSECs) and DCs. The effects of our LNP formulations on the immunological relevant NPCs population of the liver displayed an up-regulation in the expression of CD86 activation marker after treatment with LNP-CpG, LNP-MPLA and LNP-MPLA-CpG. A slight increase in activation of KC and LSECs is crucial for maintenance of liver homeostasis and the interplay between them could play an important role in immune tolerance processes in the liver [68]. It has been reported that KC could interact with LSECs *via* IP-10 to contribute to Con A-induced hepatitis [69]. This cytokine release induced by adjuvant loaded LNPs could be beneficial for a strong antiviral response by innate immunity activation [70]. In the DCs population, only activation of CD86 was observed with the LNP-MPLA-CpG formulation. In terms of cytokine release, the strong response observed for encapsulated CpG aligns with other reports on LNPs, which describe increased levels of IFN-γ toward a Th1 immune response [18,20]. Similarly to the immune activation observed in the spleen, the increase in IFN-γ, TNF-α and IP-10 reflects a robust Th1 immune response. However, unlike in the spleen, a significant elevation in CCL2, typically associated with Th2 responses, was observed in the liver suggesting a more complex and organ-specific modulation of the immune response.

In summary, the presented results demonstrated efficient mRNA translation in combination with a strong Th1-directed and pro-inflammatory cytokine response, essential characteristics for vaccines targeting viral, intracellular and parasitic pathogens. Clinically, this dual-adjuvant LNP platform holds strong potential for the development of next-generation therapeutic vaccines, particularly against chronic infections where robust, Th1-based immune responses are critical. The combination of two adjuvants, CpG and MPLA, within a LNP formulation offers a low toxicity delivery method while maintaining efficient mRNA translation, which supports translational pathways toward human clinical trials. Industrially, the formulation strategy can be applied to enhance the immunogenicity and efficacy of mRNA-based vaccines or therapeutics in large-scale manufacturing settings, taking advantage of the existing infrastructure for LNP production. In broader research contexts, this work provides a versatile platform for studying synergistic adjuvant effects, innate immune activation, and tissue-specific biodistribution of nanoparticle-based vaccines, offering new alternatives for customized immune engineering in applications ranging from infectious disease to cancer immunotherapy. Finally, it is important to mention that although the co-encapsulation of CpG and MPLA into LNPs demonstrated efficient innate immune activation both *in vitro* and *in vivo*, further studies are required to assess the long-term durability of the immune response and to evaluate the induction of robust antigen-specific immunity following an appropriate immunization scheme. Additionally, considering that the study primarily focused on DC-mediated immune responses, it would be of interest to investigate the effects on other immune cell subsets, including T and B cells. Finally, comprehensive safety profiling, along with immunogenicity and efficacy studies in a relevant disease model, will be necessary prior to clinical applications.

CRediT authorship contribution statement

Ana Pena Vaquero: Writing – review & editing, Writing – original draft, Validation, Software, Methodology, Investigation, Formal analysis, Data curation, Conceptualization. **Paula Calderon-Ruiz:** Writing – review & editing, Validation, Software, Methodology, Investigation, Formal analysis, Data curation. **Rocio Gambaro:** Writing – review & editing, Writing – original draft, Validation, Software, Methodology, Formal analysis, Conceptualization. **Ignacio Rivero-Berti:** Writing – review & editing, Writing – original draft, Validation, Software, Methodology, Formal analysis, Conceptualization. **María-José Limeres:** Writing – review & editing, Writing – original draft, Validation, Software, Methodology, Formal analysis, Conceptualization. **Silvia Fraude-El Ghazi:** Writing – original draft, Software, Methodology. **Cristián Huck-Iriart:** Validation, Software, Resources, Methodology, Formal analysis. **Claudius U. Meyer:** Writing – review & editing, Formal analysis, Conceptualization. **Maximiliano L. Cacicedo:** Writing – review & editing, Supervision, Project administration, Investigation, Formal analysis, Conceptualization. **Thomas Hankeln:** Writing – review & editing, Supervision, Conceptualization. **Shutian Si:** Validation, Software, Resources, Methodology, Funding acquisition, Formal analysis. **Ingo Lieberwirth:** Software, Resources, Methodology, Formal analysis. **Katharina Landfester:** Writing – review & editing, Resources, Formal analysis, Conceptualization. **Catalina Alba Soto:** Writing – review & editing, Writing – original draft, Supervision, Investigation, Formal analysis, Conceptualization. **Valeria Tekiel:** Writing – review & editing, Writing – original draft, Supervision, Investigation, Formal analysis, Conceptualization. **Matthias Bros:** Writing – review & editing, Writing – original draft, Supervision, Investigation, Formal analysis, Conceptualization. **Stephan Gehring:** Writing – review & editing, Writing – original draft, Supervision, Resources, Project administration, Investigation, Funding acquisition, Formal analysis, Data curation, Conceptualization. **German A. Islan:** Writing – review & editing, Writing – original draft, Supervision, Project administration, Investigation, Formal analysis, Data curation, Conceptualization.

Informed consent statement

The blood samples were obtained from the blood bank of the University Medical Center Mainz in accordance with the principles proclaimed in the Universal Declaration of Human Rights of 1948, the ethical norms established by the Nuremberg Code of 1947, and the Declaration of Helsinki of 1964 and its successive amendments and clarifications. Special attention was paid to patient rights in their relationship with health professionals and institutions and the Protection of Personal Data law.

Institutional review board statement

The animal study protocol was approved by the Institutional Review Board (or Ethics Committee) of the Landesuntersuchungsamt (LUA) Koblenz (protocol code NTP-ID: 00072130–1-8) and CICUAL (*Comité Institucional para el Uso y Cuidado de Animales de Laboratorio*) from Argentina (EX-2023-07068239- -UBA-DMEA#FMED y Res.(CD)n° 14/2014), for studies involving animals. For the isolation of splenocytes and NPCs, mice were sacrificed for organ retrieval according to § 4(3) TierSchG.

Declaration of Generative AI and AI-assisted technologies in the writing process

During the preparation of this work, the author(s) used "ChatGPT – OpenAI" and "DeepL Translate" in order to improve language and

readability. After using this tool/service, the author(s) reviewed and edited the content as needed and take(s) full responsibility for the content of the publication.

Funding

This research was funded by the Deutsche Forschungsgemeinschaft (DFG) (SFB1066, project no. B15 to M. B. and S. G.). Shutian Si also acknowledges the financial support from the DFG (SFB 1551, project no. 464588647).

Declaration of competing interest

The authors declare that they have no known competing financial interests or personal relationships that could have appeared to influence the work reported in this paper.

Acknowledgments

We appreciate the technical support contributed by Leah Pretsch, Katja Hilbert and Britta Groendahl.

Appendix A. Supplementary data

Supplementary data to this article can be found online at https://doi.org/10.1016/j.ijbiomac.2025.148058.

Data availability

The original contributions presented in the study are included in the article/supplementary material. Further inquiries can be directed to the corresponding authors.

References

[1] X. Hou, T. Zaks, R. Langer, Y. Dong, Lipid nanoparticles for mRNA delivery, Nat. Rev. Mater. 6 (2021) 1078–1094, https://doi.org/10.1038/s41578-021-00358-0.
[2] C. Hald Albertsen, J.A. Kulkarni, D. Witzigmann, M. Lind, K. Petersson, J. B. Simonsen, The role of lipid components in lipid nanoparticles for vaccines and gene therapy, Adv. Drug Deliv. Rev. 188 (2022) 114416, https://doi.org/10.1016/j.addr.2022.114416.
[3] Y. Lee, M. Jeong, J. Park, H. Jung, H. Lee, Immunogenicity of lipid nanoparticles and its impact on the efficacy of mRNA vaccines and therapeutics, Exp. Mol. Med. 55 (2023) 2085–2096, https://doi.org/10.1038/s12276-023-01086-x.
[4] K.L. Singleton, A. Joffe, W.W. Leitner, Review: current trends, challenges, and success stories in adjuvant research, Front. Immunol. 14 (2023), https://doi.org/10.3389/fimmu.2023.1105655.
[5] M. Svensson, M.J. Limeres, Y. Zeyn, R.C. Gambaro, G.A. Islan, I.R. Berti, S.F.-E. Ghazi, L. Pretsch, K. Hilbert, P. Schneider, L. Kaps, M. Bros, S. Gehring, M. L. Cacicedo, mRNA-LNP vaccine strategies: effects of adjuvants on non-parenchymal liver cells and tolerance, Mol. Ther. Methods Clin. Dev. 33 (2025), https://doi.org/10.1016/j.omtm.2025.101427.
[6] M. Fichter, M. Dedters, A. Pietrzak-Nguyen, L. Pretsch, C.U. Meyer, S. Strand, F. Zepp, G. Baier, K. Landfester, S. Gehring, Monophosphoryl lipid a coating of hydroxyethyl starch nanocapsules drastically increases uptake and maturation by dendritic cells while minimizing the adjuvant dosage, Vaccine 33 (2015) 838–846, https://doi.org/10.1016/j.vaccine.2014.12.072.
[7] T. Zhao, Y. Cai, Y. Jiang, X. He, Y. Wei, Y. Yu, X. Tian, Vaccine adjuvants: mechanisms and platforms, Signal Transduct. Target. Ther. 8 (2023) 1–24, https://doi.org/10.1038/s41392-023-01557-7.
[8] K. Kobiyama, K.J. Ishii, Making innate sense of mRNA vaccine adjuvanticity, Nat. Immunol. 23 (2022) 474–476, https://doi.org/10.1038/s41590-022-01168-4.
[9] J. Nelson, E.W. Sorensen, S. Mintri, A.E. Rabideau, W. Zheng, G. Besin, N. Khatwani, S.V. Su, E.J. Miracco, W.J. Issa, S. Hoge, M.G. Stanton, J.L. Joyal, Impact of mRNA chemistry and manufacturing process on innate immune activation, Sci. Adv. 6 (2020) eaaz6893, https://doi.org/10.1126/sciadv.aaz6893.
[10] S.G. Reed, M.T. Orr, C.B. Fox, Key roles of adjuvants in modern vaccines, Nat. Med. 19 (2013) 1597–1608, https://doi.org/10.1038/nm.3409.
[11] T. Duan, Y. Du, C. Xing, H.Y. Wang, R.-F. Wang, Toll-like receptor signaling and its role in cell-mediated immunity, Front. Immunol. 13 (2022), https://doi.org/10.3389/fimmu.2022.812774.
[12] A. Kaur, J. Baldwin, D. Brar, D.B. Salunke, N. Petrovsky, Toll-like receptor (TLR) agonists as a driving force behind next-generation vaccine adjuvants and cancer therapeutics, Curr. Opin. Chem. Biol. 70 (2022) 102172, https://doi.org/10.1016/j.cbpa.2022.102172.
[13] M. Mirshekar, S. Haghighat, Z. Mousavi, A.H. Abdolghaffari, M.H. Yazdi, Monophosphoryl lipid a as a co-adjuvant in methicillin-resistant Staphylococcus aureus vaccine development: improvement of immune responses in a mouse model of infection, Immunol. Res. 72 (2024) 490–502, https://doi.org/10.1007/s12026-024-09456-x.
[14] M. Komai-Koma, Y. Ji, H. Cao, Z. Liu, C. McSharry, D. Xu, Monophosphoryl lipid a directly regulates Th1 cytokine production in human CD4+ T-cells through toll-like receptor 2 and 4, Immunobiology 226 (2021) 152132, https://doi.org/10.1016/j.imbio.2021.152132.
[15] D.M. Klinman, Immunotherapeutic uses of CpG oligodeoxynucleotides, Nat. Rev. Immunol. 4 (2004) 249–259, https://doi.org/10.1038/nri1329.
[16] C. Bode, G. Zhao, F. Steinhagen, T. Kinjo, D.M. Klinman, CpG DNA as a vaccine adjuvant, Expert Rev. Vaccines 10 (2011) 499–511, https://doi.org/10.1586/erv.10.174.
[17] G.-H. Lee, S.-G. Lim, CpG-Adjuvanted hepatitis B vaccine (HEPLISAV-B®) update, Expert Rev. Vaccines 20 (2021) 487–495, https://doi.org/10.1080/14760584.2021.1908133.
[18] S. Shirai, M. Shibuya, A. Kawai, S. Tamiya, L. Munakata, D. Omata, R. Suzuki, T. Aoshi, Y. Yoshioka, Lipid nanoparticles potentiate CpG-Oligodeoxynucleotide-based vaccine for influenza virus, Front. Immunol. 10 (2020) 3018, https://doi.org/10.3389/fimmu.2019.03018.
[19] Z. Zhong, Y. Chen, K. Deswarte, H. Lauwers, E. De Lombaerde, X. Cui, S. Van Herck, T. Ye, M. Gontsarik, S. Lienenklaus, N.N. Sanders, B.N. Lambrecht, S. De Koker, B.G. De Geest, Lipid nanoparticle delivery alters the Adjuvanticity of the TLR9 agonist CpG by innate immune activation in lymphoid tissue, Adv. Healthc. Mater. 12 (2023) 2301687, https://doi.org/10.1002/adhm.202301687.
[20] N. Luan, H. Cao, Y. Wang, K. Lin, C. Liu, LNP-CpG ODN-adjuvanted varicella-zoster virus glycoprotein E induced comparable levels of immunity with Shingrix™ in VZV-primed mice, Virol. Sin. 37 (2022) 731–739, https://doi.org/10.1016/j.virs.2022.06.002.
[21] S. Meulewaeter, I. Aernout, J. Deprez, Y. Engelen, M. De Velder, L. Franceschini, K. Breckpot, S. Van Calenbergh, C. Asselman, K. Boucher, F. Impens, S.C. De Smedt, R. Verbeke, I. Lentacker, Alpha-galactosylceramide improves the potency of mRNA LNP vaccines against cancer and intracellular bacteria, J. Control. Release Off. J. Control. Release Soc. 370 (2024) 379–391, https://doi.org/10.1016/j.jconrel.2024.04.052.
[22] L. Pan, L. Zhang, W. Deng, J. Lou, X. Gao, X. Lou, Y. Liu, X. Yao, Y. Sheng, Y. Yan, C. Ni, M. Wang, C. Tian, F. Wang, Z. Qin, Spleen-selective co-delivery of mRNA and TLR4 agonist-loaded LNPs for synergistic immunostimulation and Th1 immune responses, J. Control. Release 357 (2023) 133–148, https://doi.org/10.1016/j.jconrel.2023.03.041.
[23] Z. Wu, K. Liu, Overview of vaccine adjuvants, Med. Drug Discov. 11 (2021) 100103, https://doi.org/10.1016/j.medidd.2021.100103.
[24] G. Mutwiri, V. Gerdts, S. van Drunen Littel-van den Hurk, G. Auray, N. Eng, S. Garlapati, L.A. Babiuk, A. Potter, Combination adjuvants: the next generation of adjuvants? Expert Rev. Vaccines 10 (2011) 95–107, https://doi.org/10.1586/erv.10.154.
[25] B. Pulendran, P.S. Arunachalam, D.T. O'Hagan, Emerging concepts in the science of vaccine adjuvants, Nat. Rev. Drug Discov. 20 (2021) 454–475, https://doi.org/10.1038/s41573-021-00163-y.
[26] S. Nazeri, S. Zakeri, A.A. Mehrizi, N.D. Djadid, G. Snounou, C. Andolina, F. Nosten, Vaccine adjuvants CpG (oligodeoxynucleotides ODNs), MPL (3-O-deacylated monophosphoryl lipid a) and naloxone-enhanced Th1 immune response to the plasmodium vivax recombinant thrombospondin-related adhesive protein (TRAP) in mice, Med. Microbiol. Immunol. (Berl.) 207 (2018) 271–286, https://doi.org/10.1007/s00430-018-0545-2.
[27] A.T. Lampe, B.L. Puniya, A.K. Pannier, T. Helikar, D.M. Brown, Combined TLR4 and TLR9 agonists induce distinct phenotypic changes in innate immunity in vitro and in vivo, Cell. Immunol. 355 (2020) 104149, https://doi.org/10.1016/j.cellimm.2020.104149.
[28] R. Gambaro, I. Rivero Berti, M.J. Limeres, C. Huck-Iriart, M. Svensson, S. Fraude, L. Pretsch, S. Si, I. Lieberwirth, S. Gehring, M. Cacicedo, G.A. Islan, Optimizing mRNA-loaded lipid nanoparticles as a potential tool for protein-replacement therapy, Pharmaceutics 16 (2024) 771, https://doi.org/10.3390/pharmaceutics16060771.
[29] B. Kim, R.R. Hosn, T. Remba, D. Yun, N. Li, W. Abraham, M.B. Melo, M. Cortes, B. Li, Y. Zhang, Y. Dong, D.J. Irvine, Optimization of storage conditions for lipid nanoparticle-formulated self-replicating RNA vaccines, J. Control. Release 353 (2023) 241–253, https://doi.org/10.1016/j.jconrel.2022.11.022.
[30] W. Rasband, ImageJ, U.S. National Institutes of Health, Bethesda, Maryland, USA. Http://Imagej.Nih.Gov/Ij/, 2011. https://cir.nii.ac.jp/crid/1570854175774652672 (accessed May 6, 2025).
[31] G. Ashiotis, A. Deschildre, Z. Nawaz, J.P. Wright, D. Karkoulis, F.E. Picca, J. Kieffer, The fast azimuthal integration Python library: *pyFAI*, J. Appl. Crystallogr. 48 (2015) 510–519, https://doi.org/10.1107/s1600576715004306.
[32] F. Sebastiani, M. Yanez Arteta, M. Lerche, L. Porcar, C. Lang, R.A. Bragg, C. S. Elmore, V.R. Krishnamurthy, R.A. Russell, T. Darwish, H. Pichler, S. Waldie, M. Moulin, M. Haertlein, V.T. Forsyth, L. Lindfors, M. Cárdenas, Apolipoprotein E Binding Drives Structural and Compositional Rearrangement of mRNA-Containing Lipid Nanoparticles, ACS Nano 15 (2021) 6709–6722, https://doi.org/10.1021/acsnano.0c10064.
[33] J.A. Welsh, D.C.I. Goberdhan, L. O'Driscoll, E.I. Buzas, C. Blenkiron, B. Bussolati, H. Cai, D. Di Vizio, T.A.P. Driedonks, U. Erdbrügger, J.M. Falcon-Perez, Q.-L. Fu, A. F. Hill, M. Lenassi, S.K. Lim, M.G. Mahoney, S. Mohanty, A. Möller, R. Nieuwland, T. Ochiya, S. Sahoo, A.C. Torrecilhas, L. Zheng, A. Zijlstra, S. Abuelreich, R. Bagabas, P. Bergese, E.M. Bridges, M. Brucale, D. Burger, R.P. Carney,

E. Cocucci, R. Crescitelli, E. Hanser, A.L. Harris, N.J. Haughey, A. Hendrix, A. R. Ivanov, T. Jovanovic-Talisman, N.A. Kruh-Garcia, V. Ku'ulei-Lyn Faustino, D. Kyburz, C. Lässer, K.M. Lennon, J. Lötvall, A.L. Maddox, E.S. Martens-Uzunova, R.R. Mizenko, L.A. Newman, A. Ridolfi, E. Rohde, T. Rojalin, A. Rowland, A. Saftics, U.S. Sandau, J.A. Saugstad, F. Shekari, S. Swift, D. Ter-Ovanesyan, J. P. Tosar, Z. Useckaite, F. Valle, Z. Varga, E. van der Pol, M.J.C. van Herwijnen, M. H.M. Wauben, A.M. Wehman, S. Williams, A. Zendrini, A.J. Zimmerman, M. Consortium, C. Théry, K.W. Witwer, Minimal information for studies of extracellular vesicles (MISEV2023): From basic to advanced approaches, J. Extracell. Vesicles 13 (2024) e12404, https://doi.org/10.1002/jev2.12404.

[34] P. Patel, N.M. Ibrahim, K. Cheng, The importance of apparent pKa in the development of nanoparticles encapsulating siRNA and mRNA, Trends Pharmacol. Sci. 42 (2021) 448–460, https://doi.org/10.1016/j.tips.2021.03.002.

[35] I. Rivero Berti, R.C. Gambaro, M.J. Limeres, C. Huck-Iriart, M. Svensson, S. Fraude-El Ghazi, L. Pretsch, S. Si, I. Lieberwirth, K. Landfester, M.L. Cacicedo, G.A. Islan, S. Gehring, Encapsulation of dexamethasone into mRNA-lipid nanoparticles is a promising approach for the development of liver-targeted anti-inflammatory therapies, Int. J. Mol. Sci. 25 (2024) 11254, https://doi.org/10.3390/ijms252011254.

[36] C. Toledo, R.C. Gambaro, G. Padula, M.E. Vela, G.R. Castro, C.Y. Chain, G.A. Islan, Binary medical Nanofluids by combination of polymeric Eudragit nanoparticles for Vehiculization of tobramycin and resveratrol: antimicrobial, Hemotoxicity and protein Corona studies, J. Pharm. Sci. 110 (2021) 1739–1748, https://doi.org/10.1016/j.xphs.2021.01.005.

[37] K.J. Hassett, K.E. Benenato, E. Jacquinet, A. Lee, A. Woods, O. Yuzhakov, S. Himansu, J. Deterling, B.M. Geilich, T. Ketova, C. Mihai, A. Lynn, I. McFadyen, M.J. Moore, J.J. Senn, M.G. Stanton, Ö. Almarsson, G. Ciaramella, L.A. Brito, Optimization of lipid nanoparticles for intramuscular administration of mRNA vaccines, Mol. Ther. Nucleic Acids 15 (2019) 1–11, https://doi.org/10.1016/j.omtn.2019.01.013.

[38] A.K.K. Leung, Y.Y.C. Tam, S. Chen, I.M. Hafez, P.R. Cullis, Microfluidic mixing: a general method for encapsulating macromolecules in lipid nanoparticle systems, J. Phys. Chem. B 119 (2015) 8698–8706, https://doi.org/10.1021/acs.jpcb.5b02891.

[39] A.K.K. Leung, Y.Y.C. Tam, S. Chen, I.M. Hafez, P.R. Cullis, Microfluidic mixing: a general method for encapsulating macromolecules in lipid nanoparticle systems, J. Phys. Chem. B 119 (2015) 8698–8706, https://doi.org/10.1021/acs.jpcb.5b02891.

[40] N. Pardi, M.J. Hogan, F.W. Porter, D. Weissman, mRNA vaccines — a new era in vaccinology, Nat. Rev. Drug Discov. 17 (2018) 261–279, https://doi.org/10.1038/nrd.2017.243.

[41] M.M.T. van Leent, B. Priem, D.P. Schrijver, A. de Dreu, S.R.J. Hofstraat, R. Zwolsman, T.J. Beldman, M.G. Netea, W.J.M. Mulder, Regulating trained immunity with nanomedicine, Nat. Rev. Mater. 7 (2022) 465–481, https://doi.org/10.1038/s41578-021-00413-w.

[42] S. Ndeupen, Z. Qin, S. Jacobsen, A. Bouteau, H. Estanbouli, B.Z. Igyártó, The mRNA-LNP platform's lipid nanoparticle component used in preclinical vaccine studies is highly inflammatory, iScience 24 (2021) 103479, https://doi.org/10.1016/j.isci.2021.103479.

[43] B. Rodenak-Kladniew, M.A. Castro, R.C. Gambaro, J. Girotti, J.S. Cisneros, S. Viña, G. Padula, R. Crespo, G.R. Castro, S. Gehring, C.Y. Chain, G.A. Islan, Cytotoxic screening and enhanced anticancer activity of Lippia alba and Clinopodium nepeta essential oils-loaded biocompatible lipid nanoparticles against lung and Colon Cancer cells, Pharmaceutics 15 (2023) 2045, https://doi.org/10.3390/pharmaceutics15082045.

[44] J. Di, Z. Du, K. Wu, S. Jin, X. Wang, T. Li, Y. Xu, Biodistribution and non-linear gene expression of mRNA LNPs affected by delivery route and particle size, Pharm. Res. 39 (2022) 105–114, https://doi.org/10.1007/s11095-022-03166-5.

[45] A. Pietrzak-Nguyen, K. Piradashvili, M. Fichter, L. Pretsch, F. Zepp, F.R. Wurm, K. Landfester, S. Gehring, MPLA-coated hepatitis B virus surface antigen (HBsAg) nanocapsules induce vigorous T cell responses in cord blood derived human T cells, nanomedicine Nanotechnol, Biol. Med. 12 (2016) 2383–2394, https://doi.org/10.1016/j.nano.2016.07.010.

[46] E. Dollinger, J. Hernandez-Davies, J. Felgner, A. Jain, M. Hwang, E. Strahsburger, R. Nakajima, A. Jasinskas, Q. Nie, E.J. Pone, S. Othy, D.H. Davies, Combination adjuvant improves influenza virus immunity by downregulation of immune homeostasis genes in lymphocytes, ImmunoHorizons 9 (2025) vlae007, https://doi.org/10.1093/immhor/vlae007.

[47] E.-J. Ko, Y. Lee, Y.-T. Lee, Y.-J. Kim, K.-H. Kim, S.-M. Kang, MPL and CpG combination adjuvants promote homologous and heterosubtypic cross protection of inactivated split influenza virus vaccine, Antivir. Res. 156 (2018) 107–115, https://doi.org/10.1016/j.antiviral.2018.06.004.

[48] R. Augustine, A. Hasan, R. Primavera, R.J. Wilson, A.S. Thakor, B.D. Kevadiya, Cellular uptake and retention of nanoparticles: insights on particle properties and interaction with cellular components, Mater Today Commun 25 (2020) 101692, https://doi.org/10.1016/j.mtcomm.2020.101692.

[49] S. Bhattacharjee, DLS and zeta potential – what they are and what they are not? J. Control. Release 235 (2016) 337–351, https://doi.org/10.1016/j.jconrel.2016.06.017.

[50] M.H.Y. Cheng, J. Leung, Y. Zhang, C. Strong, G. Basha, A. Momeni, Y. Chen, E. Jan, A. Abdolahzadeh, X. Wang, J.A. Kulkarni, D. Witzigmann, P.R. Cullis, Induction of bleb structures in lipid nanoparticle formulations of mRNA leads to improved transfection potency, Adv. Mater. 35 (2023) 2303370, https://doi.org/10.1002/adma.202303370.

[51] M.L. Cacicedo, C. Weinl-Tenbruck, D. Frank, S. Wirsching, B.K. Straub, J. Hauke, J. G. Okun, N. Horscroft, J.B. Hennermann, F. Zepp, F. Chevessier-Tünnesen, S. Gehring, mRNA-based therapy proves superior to the standard of care for treating hereditary tyrosinemia 1 in a mouse model, Mol. Ther. Methods Clin. Dev. 26 (2022) 294–308, https://doi.org/10.1016/j.omtm.2022.07.006.

[52] Y. Granot, D. Peer, Delivering the right message: challenges and opportunities in lipid nanoparticles-mediated modified mRNA therapeutics—an innate immune system standpoint, Semin. Immunol. 34 (2017) 68–77, https://doi.org/10.1016/j.smim.2017.08.015.

[53] A. Muslimov, V. Tereshchenko, D. Shevyrev, A. Rogova, K. Lepik, V. Reshetnikov, R. Ivanov, The dual role of the innate immune system in the effectiveness of mRNA therapeutics, Int. J. Mol. Sci. 24 (2023) 14820, https://doi.org/10.3390/ijms241914820.

[54] R.R. Rapaka, A.S. Cross, M.A. McArthur, Using adjuvants to drive T cell responses for next-generation infectious disease vaccines, Vaccines 9 (2021) 820, https://doi.org/10.3390/vaccines9080820.

[55] J. Hoge, I. Yan, N. Jänner, V. Schumacher, A. Chalaris, O.M. Steinmetz, D.R. Engel, J. Scheller, S. Rose-John, H.-W. Mittrücker, IL-6 controls the innate immune response against Listeria monocytogenes via classical IL-6 signaling, J. Immunol. 190 (2013) 703–711, https://doi.org/10.4049/jimmunol.1201044.

[56] L. Velazquez-Salinas, A. Verdugo-Rodriguez, L.L. Rodriguez, M.V. Borca, The role of interleukin 6 during viral infections, Front. Microbiol. 10 (2019) 1057, https://doi.org/10.3389/fmicb.2019.01057.

[57] C. Dong, Cytokine regulation and function in T cells, Annu. Rev. Immunol. 39 (2021) 51–76, https://doi.org/10.1146/annurev-immunol-061020-053702.

[58] S. Shirai, M. Shibuya, A. Kawai, S. Tamiya, L. Munakata, D. Omata, R. Suzuki, T. Aoshi, Y. Yoshioka, Lipid nanoparticles potentiate CpG-Oligodeoxynucleotide-based vaccine for influenza virus, Front. Immunol. 10 (2020), https://doi.org/10.3389/fimmu.2019.03018.

[59] F.H.N. Howard, A. Kwan, N. Winder, A. Mughal, C. Collado-Rojas, M. Muthana, Understanding immune responses to viruses—do underlying Th1/Th2 cell biases predict outcome? Viruses 14 (2022) 1493, https://doi.org/10.3390/v14071493.

[60] J. Muller-Berghaus, W.C. Olson, R.A. Moulton, W.T. Knapp, D. Schadendorf, W. J. Storkus, IL-12 production by human monocyte-derived dendritic cells: looking at the single cell, J. Immunother. Hagerstown Md 1997 (28) (2005) 306–313, https://doi.org/10.1097/01.cji.0000163594.74533.10.

[61] B.M. Carreno, M. Becker-Hapak, A. Huang, M. Chan, A. Alyasiry, W.-R. Lie, R. L. Aft, L.A. Cornelius, K.M. Trinkaus, G.P. Linette, IL-12p70-producing patient DC vaccine elicits Tc1-polarized immunity, J. Clin. Invest. 123 (2013) 3383–3394, https://doi.org/10.1172/JCI68395.

[62] H.-I. Hung, O.J. Klein, S.W. Peterson, S.R. Rokosh, S. Osseiran, N.H. Nowell, C. L. Evans, PLGA nanoparticle encapsulation reduces toxicity while retaining the therapeutic efficacy of EtNBS-PDT in vitro, Sci. Rep. 6 (2016) 33234, https://doi.org/10.1038/srep33234.

[63] I. Pateev, K. Seregina, R. Ivanov, V. Reshetnikov, Biodistribution of RNA vaccines and of their products: evidence from human and animal studies, Biomedicines 12 (2024) 59, https://doi.org/10.3390/biomedicines12010059.

[64] X. He, J. Wang, Y. Tang, S.T. Chiang, T. Han, Q. Chen, C. Qian, X. Shen, R. Li, X. Ai, Recent advances of emerging spleen-targeting Nanovaccines for immunotherapy, Adv. Healthc. Mater. 12 (2023) e2300351, https://doi.org/10.1002/adhm.202300351.

[65] M.Y. Zanna, A.R. Yasmin, A.R. Omar, S.S. Arshad, A.R. Mariatulqabtiah, S.H. Nur-Fazila, M.I.N. Mahiza, Review of dendritic cells, their role in clinical immunology, and distribution in various animal species, Int. J. Mol. Sci. 22 (2021) 8044, https://doi.org/10.3390/ijms22158044.

[66] M.A. Tam, U.A. Wenzel, M.J. Wick, Plasmacytoid dendritic cells mature independently of MyD88 and IFN-αβR in response to *Listeria* and stimulate CD8 T cells, Immunol. Lett. 138 (2011) 104–112, https://doi.org/10.1016/j.imlet.2011.03.007.

[67] M.L. Cacicedo, M.J. Limeres, S. Gehring, mRNA-based approaches to treating liver diseases, Cells 11 (2022) 3328, https://doi.org/10.3390/cells11203328.

[68] L.M. Casey, K.R. Hughes, M.N. Saunders, S.D. Miller, R.M. Pearson, L.D. Shea, Mechanistic contributions of Kupffer cells and liver sinusoidal endothelial cells in nanoparticle-induced antigen-specific immune tolerance, Biomaterials 283 (2022) 121457, https://doi.org/10.1016/j.biomaterials.2022.121457.

[69] S. Dai, F. Liu, Z. Qin, J. Zhang, J. Chen, W.-X. Ding, D. Feng, Y. Ji, X. Qin, Kupffer cells promote T-cell hepatitis by producing CXCL10 and limiting liver sinusoidal endothelial cell permeability, Theranostics 10 (2020) 7163–7177, https://doi.org/10.7150/thno.44960.

[70] M. Pimkova Polidarova, L. Vanekova, P. Brehova, M. Dejmek, Z. Vavrina, G. Birkus, A. Brazdova, Synthetic stimulator of interferon genes (STING) agonists induce a cytokine-mediated anti-hepatitis B virus response in nonparenchymal liver cells, ACS Infect. Dis. 9 (2023) 23–32, https://doi.org/10.1021/acsinfecdis.2c00424.